Measuring the Neutral Pion Polarizability

Proposal Submitted to PAC 48

overleaf as of Mon 15 Jun 2020 08:45:39 PM EDT

M.M. Ito*[1], D. Lawrence[1], E.S. Smith†[1], B. Zihlmann*[1], R. Miskimen*[3], I. Larin*[3], A. Austregesilo[5], D. Hornidge[6], and P. Martel[7]

[1] *Thomas Jefferson National Accelerator Facility, Newport News, VA*
[3] *University of Massachusetts, Amherst, MA*
[5] *Carnegie Mellon University, Pittsburgh, PA*
[6] *Mount Allison University, Sackville, New Brunswick, Canada*
[7] *Institute for Nuclear Physics, Johannes Gutenberg University, Mainz, Germany*

June 12, 2020

Theoretical Support

J. Goity, *Thomas Jefferson National Accelerator Facility, Newport News, Virginia and Hampton University, Hampton, Virginia*
A. Aleksejevs, *Memorial University of Newfoundland, Corner Brook, Canada*
S. Barkanova, *Memorial University of Newfoundland, Corner Brook, Canada*
S. Gevorkyan, *Joint Institute for Nuclear Research, Dubna, Russia*
L.-Y. Dai, *Hunan University, Changsha, Hunan, China*

*Spokesperson
†Contact and Spokesperson, email: elton@jlab.org

Abstract

This proposal presents our plan to make a precision measurement of the cross section for $\gamma\gamma \to \pi^0\pi^0$ via the Primakoff effect using the GlueX detector in Hall D. The aim is to significantly improve the data in the low $\pi^0\pi^0$ invariant mass domain, which is essential for understanding the low-energy regime of Compton scattering on the π^0. In particular, the aim is to obtain a first-ever experimental determination of the neutral pion polarizability $\alpha_\pi - \beta_\pi$, which is one of the important predictions of chiral perturbation theory and a key test of chiral dynamics. Our goal is to measure $\sigma(\gamma\gamma \to \pi^0\pi^0)$ to a precision of about 5.1%, which will determine the combination of $\alpha_{\pi^0} - \beta_{\pi^0}$ to a precision of 39%. We expect this experiment to run concurrently with the previously approved experiment to measure the charged pion polarizability (CPP) [1] in Hall D.

Contents

1 Introduction

Electromagnetic polarizabilities are fundamental properties of composite systems such as molecules, atoms, nuclei, and hadrons [2]. Whereas form factors provide information about the ground state properties of a system, polarizabilities provide information about the excited states of the system, and are therefore determined by the system's dynamics. Measurements of hadron polarizabilities provide an important test of Chiral Perturbation Theory, dispersion relation approaches, and lattice calculations. Among the hadron polarizabilities, the neutral pion polarizability is important because it tests fundamental symmetries, in particular chiral symmetry and its realization in QCD. Indeed, the non-trivial (non-perturbative) vacuum properties of QCD result in the phenomenon of spontaneous chiral symmetry breaking, giving rise to the Goldstone boson nature of the pions. In particular, the Goldstone boson nature of the π^0 manifests itself most notably in its decay into $\gamma\gamma$ and also in its electromagnetic polarizability, which according to ChPT can be predicted to leading order in the expansion in quark masses.

Hadron polarizabilities are best measured in Compton scattering experiments where, in the case of nucleon polarizabilities, one looks for a deviation of the cross section from the prediction of Compton scattering from a structureless Dirac particle. In the case of pions, the long lifetime of the charged pion permits experiments of low energy Compton scattering using a beam of high energy pions scattering on atomic electrons. On the other hand, the short lifetime of the neutral pion requires an indirect study of low energy Compton scattering via measurements of the process $\gamma\gamma \to \pi^0\pi^0$, a method that can also be applied to the charged pion (CPP) and for which a proposal in Hall D is already approved [1].

Measurements of hadron polarizabilities are among the most difficult experiments performed in photo-nuclear physics. For charged hadrons, because of the Born term, the polarizability effect in the cross section can range from 10 to 20% depending on the kinematics. For neutral hadrons, where the Born term is absent, the polarizability effect will be much less than this. To set reasonable expectations for what can be accomplished in a measurement of this type, it is important to recognize that after 30 years of dedicated experiments using tagged photons at facilities across North America and Europe, the error on the proton electric polarizability is 4%, without doubt the paramount experimental achievement in this field. However, the error on the proton magnetic polarizability is 16% [3]. Absolute uncertainties provide a better gauge of a measurements sensitivity; for proton electric and magnetic polarizabilities the uncertainty in both is $\pm 0.4 \times 10^{-4}$ fm^3. Another level of precision to consider for setting expectations is the result COMPASS obtained for charged pion $\alpha - \beta$. COMPASS achieved a relative error of 46% in $\alpha - \beta$ and an absolute error of $\pm 0.9 \times 10^{-4}$ fm^3. This is also a Primakoff measurement. We note that COMPASS cannot measure the neutral pion polarizability.

This proposal presents a plan to make a precision measurement of the $\gamma\gamma^* \to \pi^0\pi^0$ cross section using the GlueX detector in Hall D. The measurement is based on the Primakoff effect

which allows one to access the low $W_{\pi^0\pi^0}$ invariant mass regime with the virtual photon γ^* provided by the Coulomb field of the target. The central aim of the measurement is to drastically improve the determination of the cross section in this domain, which is key for constraining the low energy Compton amplitude of the π^0 and thus for extracting its polarizability. At present, the only accurate measurements exist for invariant masses of the two π^0s above 0.7 GeV, far above the threshold of 0.27 GeV. The existing data at low energy were obtained in $e^+e^- \to \pi^0\pi^0$ scattering in the early 1990's with the Crystal Ball detector at the DORIS-II storage ring at DESY [4].

Theory has made significant progress over time, with studies of higher chiral corrections [5, 6, 7] and with the implementation of dispersion theory analyses which serve to make use of the higher energy data [8, 9, 10, 11]. It is expected that the experimental data from this proposal, together with these theoretical frameworks, will allow for the extraction of the π^0 polarizability for the first time.

2 Theoretical predictions for the neutral pion polarizability

The low energy properties of pions are largely determined by their nature as the Goldstone Bosons of spontaneously broken chiral symmetry in QCD, and are described in a model independent way by the framework of Chiral Perturbation Theory (ChPT) (Gasser and Leutwyler [12]), which implements a systematic expansion in low energy/momentum and in quark masses. In particular the pions' low energy electromagnetic properties can serve as tests of their Goldstone Boson (GB) nature. One such case is the decay $\pi^0 \to \gamma\gamma$, which tests, at the same time, its GB nature and the chiral anomaly. Another case is low energy Compton scattering on pions: at low energy the Compton differential cross section can be expanded in powers of the photon energy and expressed in terms of the corresponding pion charge form factor (for charged pion) and the electric and magnetic polarizabilities, where the latter give the order ω^2 terms in the Compton cross section, where ω is the photon energy. The polarizabilities appear as deviations of the pions from point like particles, and thus are the result of carrying out the chiral expansion to next-to-leading order. For both charged and neutral pions the polarizabilities are fully predicted at leading order in quark masses, and thus represent a sensitive test of chiral dynamics. For the charged pions, at $O(p^4)$, ChPT predicts that the electric and magnetic polarizabilities (α_{π^+} and β_{π^+}) are related to the charged pion weak form factors F_V and F_A in the decay $\pi^+ \to e^+\nu\gamma$

$$\alpha_{\pi^+} = -\beta_{\pi^+} \propto \frac{F_A}{F_V} = \frac{1}{6}(l_6 - l_5), \tag{1}$$

where l_5 and l_6 are low energy constants in the Gasser and Leutwyler effective Lagrangian [12]. Using recent results from the PIBETA collaboration for F_A and F_V [13], the $O(p^4)$ ChPT prediction

for the charged pion electric and magnetic polarizabilities is given by:

$$\alpha_{\pi^+} = -\beta_{\pi^+} = (2.78 \pm 0.1) \times 10^{-4} \text{ fm}^3. \tag{2}$$

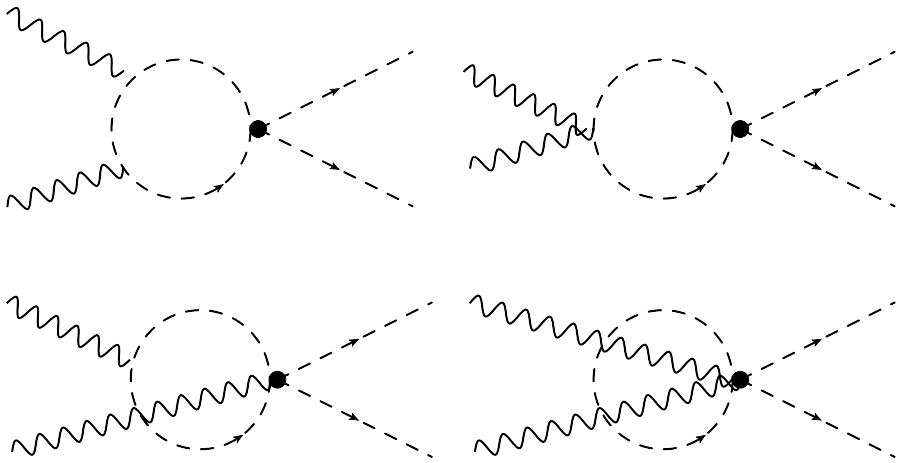

Figure 1: Diagrams contributing to Compton scattering off the π^0.

In the case of the neutral pion, the polarizabilities are determined by the one loop chiral contributions (see Fig. 1) which are calculable and free of unknown parameters. They are given in terms of only the fine structure constant, the pion mass, and the pion decay constant:

$$\begin{aligned} \alpha_{\pi^0} + \beta_{\pi^0} &= 0 \\ \alpha_{\pi^0} - \beta_{\pi^0} &= -\frac{\alpha}{48\pi^2 M_\pi F_\pi^2} \simeq -1.1 \times 10^{-4} \text{ fm}^3 \end{aligned} \tag{3}$$

However, there is a range of predictions beyond NLO and the experimental test of these important predictions is very challenging. In particular, the polarizabilities drive the very low energy regime of Compton scattering on the π^0 as there is no Thomson term, so one would expect that it would be easier to determine them than in the charged pion case. However, direct Compton scattering on the π^0 is experimentally inaccessible due to its short lifetime, and therefore it is necessary to resort to the process $\gamma\gamma \to \pi^0\pi^0$ of this proposal. In addition, ChPT indicates that the polarizabilities are smaller in the case of the neutral pion, about a third of their value for the charged pion, i.e., somewhere between -1.7×10^{-4} fm^3 and -1.9×10^{-4} fm^3, depending on the model used to estimate higher order effects in the chiral expansion. The challenge is therefore to measure the cross section for $\gamma\gamma \to \pi^0\pi^0$ with sufficient accuracy at low invariant mass $W_{\pi\pi}$ so that one can infer the low-energy Compton amplitude and extract the polarizabilities. Accuracy is required to allow for the extrapolation of the Compton amplitude from the kinematics of $\gamma\gamma \to \pi^0\pi^0$ to low energy Compton scattering, something that is at present impossible with the poor accuracy of the only available data from the Crystal Ball experiment [4].

For this purpose, the theoretical foundations have been laid in works studying $\gamma\gamma \to \pi^0\pi^0$ using both ChPT (Bellucci et al [14, 5], Gasser et al. [6], Aleksejevs and Barkanova [7]) and dispersion theory (Oller and Roca [8], Dai and Pennington [9, 10], Moussallam [11]). In particular, in ChPT at the next-to-next to leading order, which provides the higher order quark mass corrections to the polarizabilities, some of the low energy constants need to be fixed and for that a significantly more accurate measurement of the $\gamma\gamma \to \pi^0\pi^0$ cross section is needed than presently available.

Accurate measurements of the cross section near threshold combined with data for $W_{\pi\pi} > 0.6$ GeV will provide the necessary input for performing a full theoretical analysis, combining dispersion theory with and without inputs from ChPT at low energy. This is a well established method which has been used to analyze $\pi\pi$ scattering and also to this very problem, that of the $\gamma\gamma \to \pi^0\pi^0$ process, where numerous works have been steadily improving the theoretical dispersive analysis [15, 16, 8, 11, 17]. Through such an analysis it will be possible to determine, via combination with ChPT, the low energy Compton amplitude and extract the value of $\alpha_\pi - \beta_\pi$. The latter extraction represents a challenge as shown in Fig. 2, where the polarizabilities have a small direct effect on $\gamma\gamma \to \pi\pi$. Calculations by Dai and Pennington (Table II) [17] indicate that a 1.3% determination of $\sigma(\gamma\gamma \to \pi^0\pi^0)$ will determine the combination of $\alpha_{\pi^0} - \beta_{\pi^0}$ to a precision of 10%. In general, the determination of the accuracy one can get for $\alpha_\pi - \beta_\pi$ based on a more accurate measurement, like the one proposed here, is still an issue being currently studied theoretically. J. L. Goity, A. Aleksejevs, S. Barkanova, S. Gevorgyan, and L.-Y. Dai have formed a group to work on the project. At present a theoretical study based on the S-wave dominance below $W_{\pi\pi} \sim 0.8$ GeV and dispersion theory allows representation of the two Compton amplitudes A and B in the physical domain of the experiment. The study of the extrapolation to low energy Compton kinematics is under study, in particular the issues related to the stability of the dispersive analysis. This study is expected to provide a more accurate estimate on the sensitivity with which the experiment will be able to determine the polarizability $\alpha - \beta$.

3 Past measurements

Past measurements of the $\gamma\gamma \to \pi^0\pi^0$ cross section are shown in Fig. 3 and with theoretical curves in Fig. 2. The data can be summarized as follows:

1. In the early 1990's measurements were made in e^+e^- collisions at DESY with the Crystal Ball detector at the DORIS-II storage ring [4], which are the only available data for $W_{\pi\pi} < 0.6$ GeV.

2. In 2008-2009, measurements were carried out by BELLE for 0.6 GeV $< W_{\pi\pi} <$ 4.0 GeV [18, 19, 20]. Two data sets were produced with different selection cuts on $|\cos\theta^*|$.

As mentioned above, several works have made use of dispersion theory methods applied to these

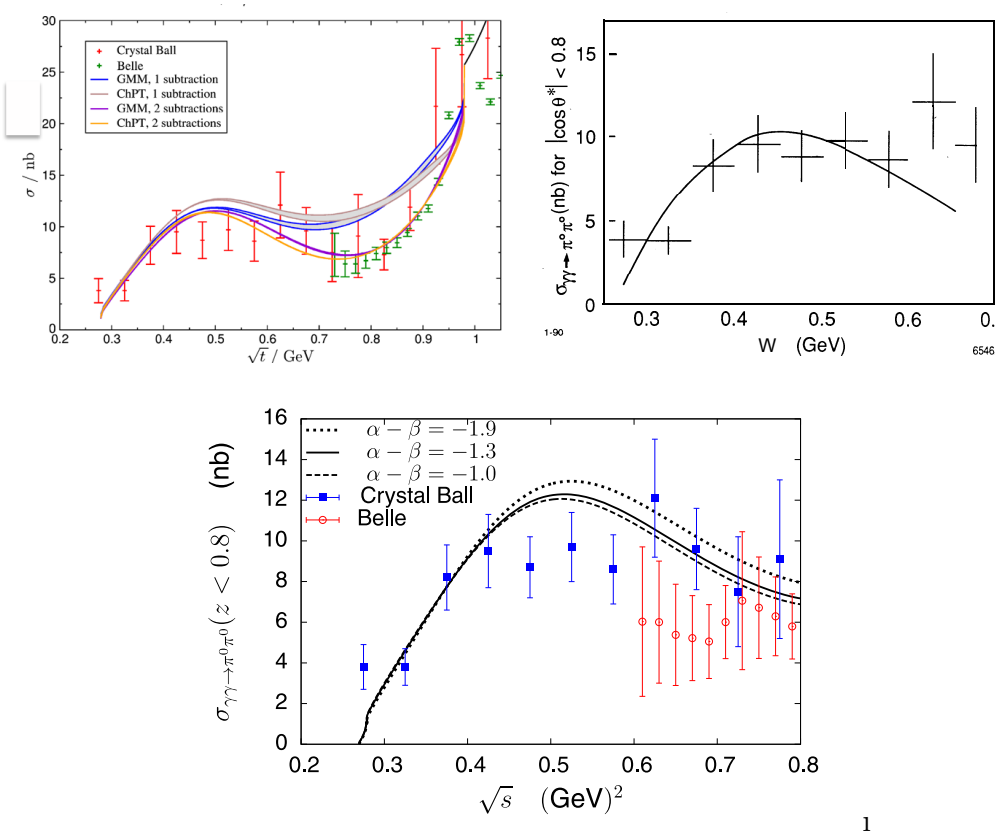

Figure 2: Left panel: experimental status; right panel: results from the 1990 XBall experiment. The lower panel shows the effect of π^0 polarizabilities on the cross section ($\sqrt{s} = W_{\pi\pi}$) [11] .

data. They include Oller and Roca [8], Dai and Pennington [17], and in particular Moussallam [11] who performed the dispersive analysis where one of the photons has non-vanishing virtuality, which is particularly important for our case. These methods give results for the cross section at small $W_{\pi\pi}$, but the poor accuracy of the data in that region does not serve as a useful constraint that could improve those analyses. On the other hand, the ChPT calculations carried out at NNLO (Bellucci et al. [14, 5]) can only be fit to the low $W_{\pi\pi}$ data, and thus the uncertainty in the determination of low energy constants is rather large. It is therefore expected that accurate data at low $W_{\pi\pi} < 0.6$ GeV will have a very big impact on both theoretical approaches, which together may allow for an accurate description of the low energy Compton amplitude, and for a experimental determination of the polarizability for the first time.

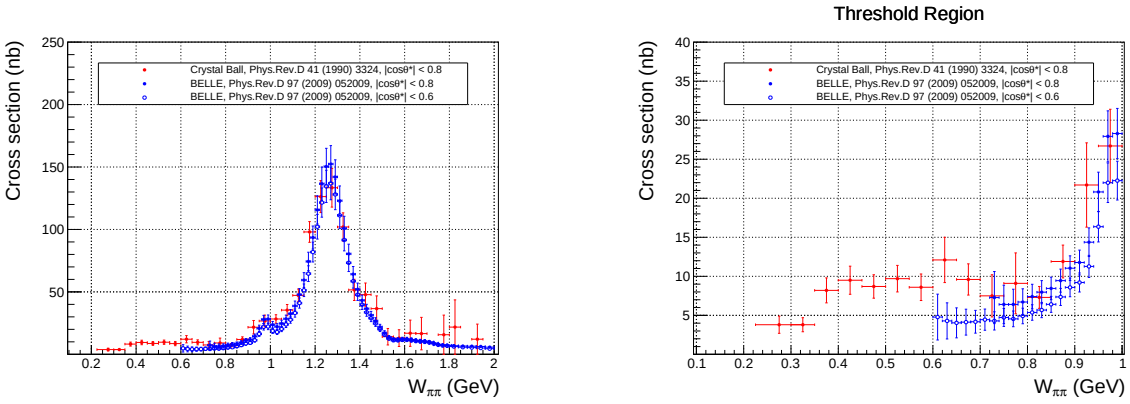

Figure 3: Data from Crystal Ball and BELLE. There are two data samples from BELLE experimental with different selection on $|\cos\theta^*|$. Left) Full range of $W_{\pi\pi}$. Right) Threshold region.

4 Experimental conditions

The measurement of the neutral pion polarizability is expected to run concurrently with the experiment to measure the charged pion polarizability (CPP) [1] in Hall D. Essentially all the optimizations for that experiment are expected to improve the sensitivity of this experiment also. We briefly summarize the configuration for CPP, which is compared in Table 1 to nominal GlueX running.

The diamond radiator will be adjusted to set the coherent peak of the photon beam between 5.5 and 6.0 GeV. This enhances the polarization significantly and also the tagging ratio compared to nominal GlueX conditions. The experimental target will be placed upstream of the nominal GlueX target by 64 cm (z=1 cm in the Hall D coordinate system). These changes benefit the present experiment. In addition, the CPP experiment will add multi-wire proportional chambers downstream for muon identification, but these do not have an impact on this measurement.

4.1 Expected signal

In order to estimate rates, resolution and acceptance due to the Primakoff reaction on lead, $\gamma^{208}\mathrm{Pb} \to \pi^0\pi^0\,\mathrm{Pb}$, we take the reaction process to be the same as for charged pion production and given in Eq. 8 of the Proposal for the Charged Pion Polarizability experiment [1], which is reproduced here for convenience:

$$\frac{d^2\sigma}{d\Omega_{\pi\pi}dW_{\pi\pi}} = \frac{2\alpha Z^2}{\pi^2}\frac{E_\gamma^4\beta^2}{W_{\pi\pi}}\frac{\sin^2\theta_{\pi\pi}}{Q^4}|F(Q^2)|^2\sigma(\gamma\gamma\to\pi^0\pi^0)(1+P_\gamma\cos 2\phi_{\pi\pi}). \quad (4)$$

Table 1: Configuration of the CPP experiment compared to nominal GlueX. We propose that this experiment run concurrently with CPP. Detectors not identified in the table are assumed to be operated under the same conditions as in the nominal configuration.

Configuration	GlueX I	CPP/NPP
Electron beam energy	11.6 GeV	11.6 GeV
Emittance	10^{-8}m rad	10^{-8}m rad
Electron current	150 nA	20 nA
Radiator thickness	50μm	50 μm diamond
Coherent peak	8.4 – 9.0 GeV	5.5 – 6.0 GeV
Collimator aperture	5 mm	5 mm
Peak polarization	35%	72%
Tagging ratio	0.6	0.72
Flux 5.5-6.0 GeV		11 MHz
Flux 8.4-9.0 GeV	20 MHz	
Flux 0.3-11.3 GeV	367 MHz	74 MHz
Target position	65 cm	1 cm
Target, length	H, 30 cm	^{208}Pb, 0.028 cm
Start counter	nominal	removed
Muon identification	None	Behind FCAL

The $\gamma\gamma$ cross section for charged pions has been substituted with the cross section for neutral pions, namely $\sigma(\gamma\gamma \to \pi^0\pi^0)$. In this expression, $\Omega_{\pi\pi}$ is the solid angle in the laboratory frame for the emission of the $\pi\pi$ system, $W_{\pi\pi}$ is the $\pi\pi$ invariant mass, Z is the atomic number of the target, β is the velocity of the $\pi\pi$ system, E_γ is the energy of the incident photon, $F(Q^2)$ is the electromagnetic form factor for the target with final-state-interaction (FSI) corrections applied, $\theta_{\pi\pi}$ is the lab angle for the $\pi\pi$ system, $\phi_{\pi\pi}$ is the azimuthal angle of the $\pi\pi$ system relative to the incident photon polarization, and P_γ is the incident photon polarization.[1]

The cross section for $\sigma(\gamma\gamma \to \pi^0\pi^0)$ has been measured by the Crystal Ball Collaboration [4], albeit with limited statistical precision. We have parameterized the cross section for $W_{\pi\pi} < 0.8$ GeV, which is of specific interest to this program as shown in Fig. 4. Using this parameterization and Eq. 4, we can calculate the photoproduction cross section on lead, which is shown in Fig. 5. The integrated cross section is 0.30 ± 0.05 μb/nucleus. The uncertainty comes from the model dependence and was obtained by comparing two different calculations using completely different parameterizations for the nuclear form factor on lead, $F(Q^2)$. For reference, we note that the cross

[1]The expression for the cross section in terms of invariant quantities can be found in Ref. [21].

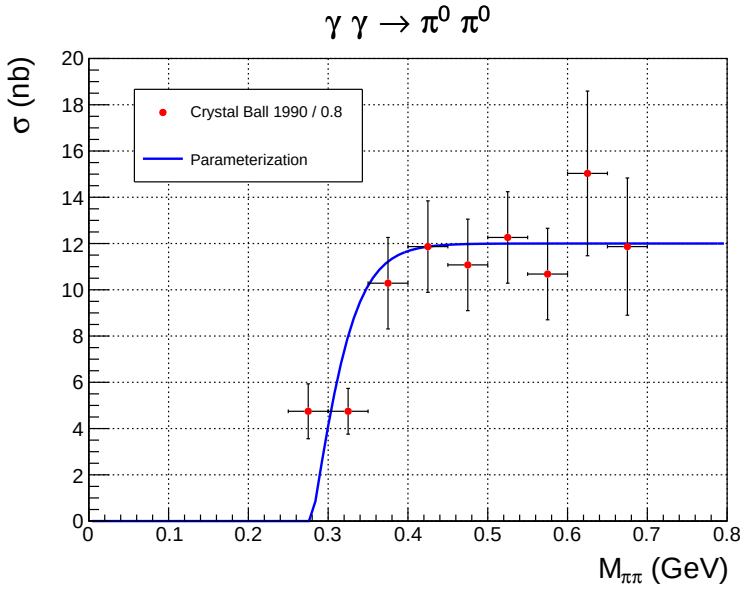

Figure 4: Parameterization of the $\sigma(\gamma\gamma \rightarrow \pi^0\pi^0)$ cross section as a function of the 2π invariant mass compared to the data from Crystal Ball [4].

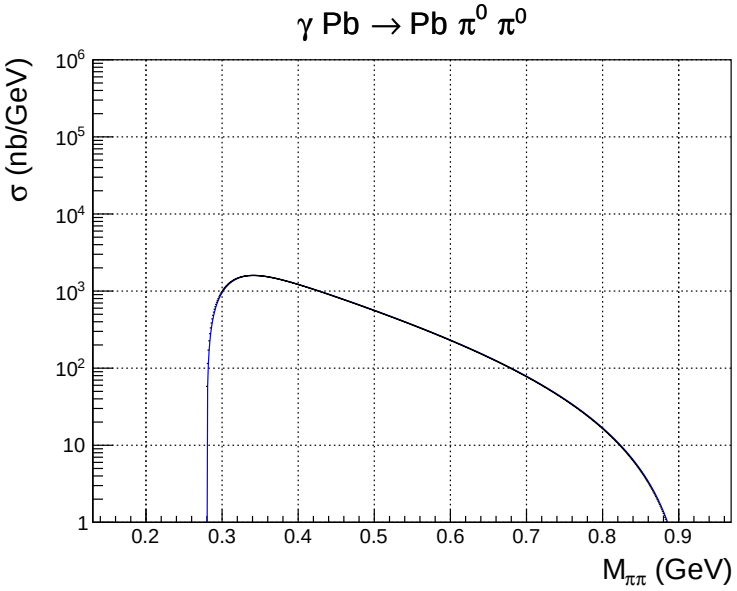

Figure 5: Primakoff cross section for $\gamma Pb \rightarrow Pb\,\pi^0\pi^0$ using the parameterization of $\sigma(\gamma\gamma \rightarrow \pi^0\pi^0)$ in the previous figure. The integrated cross section is $0.3\,\mu$b/nucleus.

section for charged pions ($\pi^+\pi^-$) production is 10.9 μb, a factor of 30 larger.

The number of neutral-pion-Primakoff-signal events produced during 20 PAC days is shown in Fig. 6. The impacts of detector trigger, acceptance and resolution are discussed in the next section.

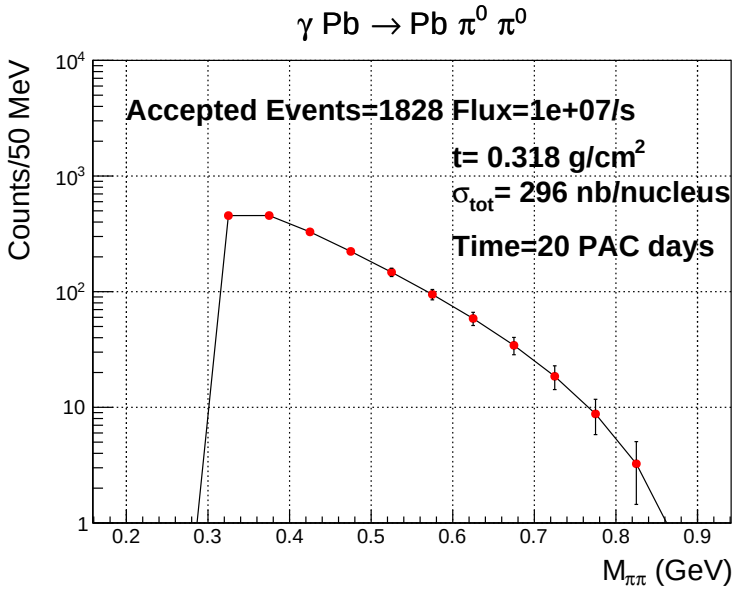

Figure 6: Estimated production rate for γPb $\rightarrow \pi^0\pi^0$ Pb as a function 2π mass. For this calculation, it is assumed the detector has perfect resolution and has a linearly increasing efficiency from zero at threshold up to 0.4 at 0.34 GeV (see top right of Fig. 13).

4.2 Detector resolution

The response of the GlueX detector to neutral pion Primakoff events was simulated using the standard GlueX generation and reconstruction tools, but with the specific geometry for the CPP experiment. The schematic of the detector configuration is shown in Fig. 7. The primary differences between the standard GlueX geometry and CPP are summarized in Table 1. For this experiment, the main differences include a) coherent peak position at 5.5-6 GeV and re-positioning of the microscope to cover the coherent peak, b) solid ^{208}Pb at z=1cm, and c) Start counter removed. For the CPP experiment, the addition of muon identification chambers behind the FCAL is critical. However, for neutral pions this addition plays no role because the photons are detected in the FCAL. The GEANT4 simulation,[2] which is used for these studies, includes most changes except

[2]The initial simulations used GEANT3 and show similar results.

for the addition of the muon chambers, which are not needed. In addition, the microscope geometry has not been modified and we use the tagger hodoscope for the region of interest in the simulation. The slightly reduced energy of the hodoscope relative to the microscope has little impact and the gaps between counters are ignored when simulating the tagged flux.

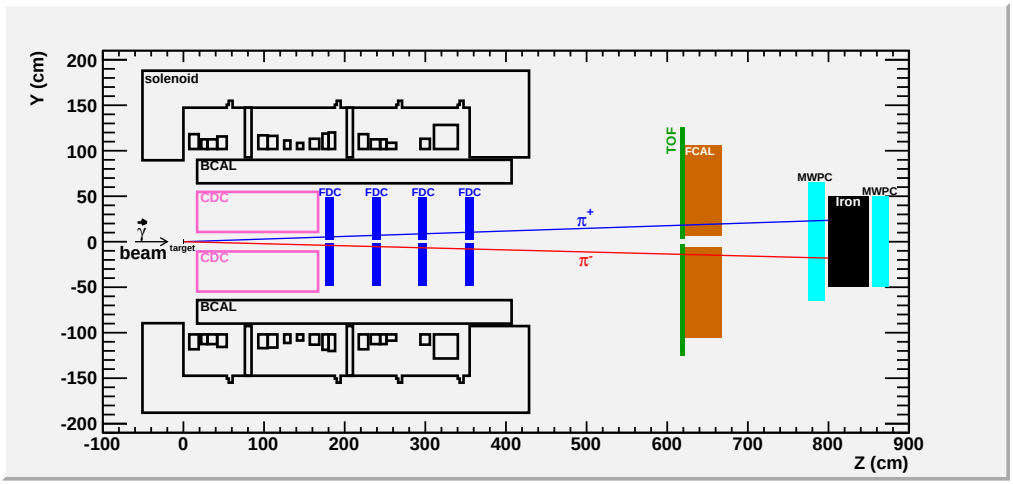

Figure 7: Diagram of the GlueX detector including the additional muon chambers for the CPP experiment.

The Primakoff signal was generated according to the cross section described in the previous chapter, using the *gen_2pi0_primakoff* program, which is a modified version of the CPP event generator. By default, the production amplitudes are symmetrized between the two identical π^0's by AmpTools. One hundred thousand events of Primakoff and nuclear coherent interactions (see Section 5.1) were generated with $M_{\pi\pi}$ <0.9 GeV. We used random triggers from run 30401[3] to add tagger accidentals and random hits in the drift chambers. These events were fed to GEANT4 to track particles, and subsequently processed using *mcsmear* to simulate the detector response. The simulated events were then analyzed using the GlueX event filter to analyze the reaction $\gamma Pb \to \pi^0\pi^0$ with a missing Pb nucleus and to constrain the detected photon pairs to the π^0 mass. Energy and momentum conservation is imposed on the reaction as well as the requirement that all photons originate from a common vertex. The output of the reconstruction, both kinematically fit and "measured" quantities, were available for inspection.

In the following we show various reconstructed quantities as well as estimated resolutions. The distribution of generated photon energy and the unconstrained reconstructed momenta of the two pions are shown in Fig. 8. The missing mass, 2π mass and $-t$ distributions are shown in Fig. 9. The reconstructed momentum relative to its generated value is shown in Fig. 10. The central peak

[3]Run 30401 is a low-intensity run for GlueX, but represents considerably higher background than expected

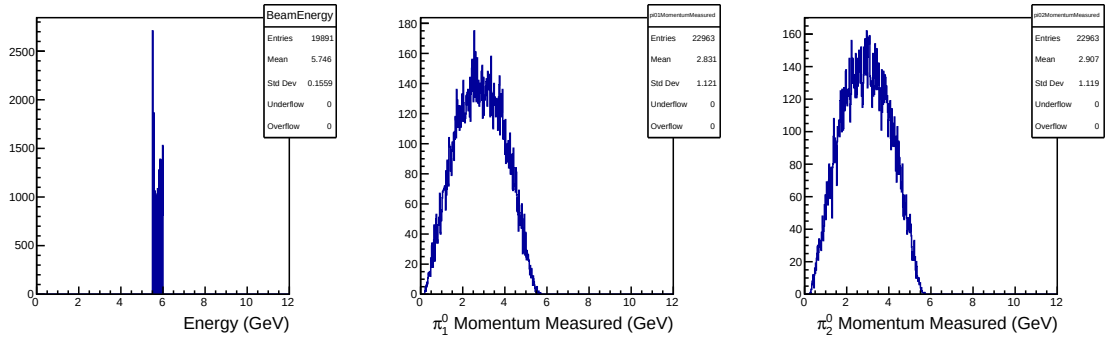

Figure 8: Left: Generated photon energies. The increased rate near 5.5 GeV is due to tagger accidentals. Center: Reconstructed momentum distribution of one π^0. Right: Reconstructed momentum distribution of the second π^0.

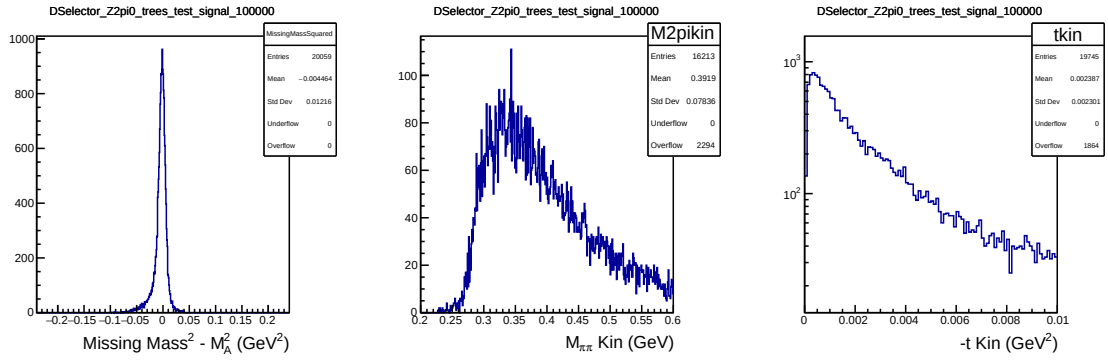

Figure 9: Left: Missing mass distribution minus the mass of the recoil nucleus. Center: Kinematically fit 2π mass distribution. Right: Kinematically fit $-t$ distribution.

of the kinematically fit momentum is about 2%, similar to that for charged pions. However, there are long tails that will effect the final reconstruction. The resolution of the azimuthal angle, $\phi_{\pi\pi}$, between the production and the photon polarization planes is quite poor owing to the fact that the pion pairs are produced at very shallow angles. Nevertheless it is sufficient to measure the asymmetry due to the photon beam polarization. The resolution of the 2π invariant mass is shown

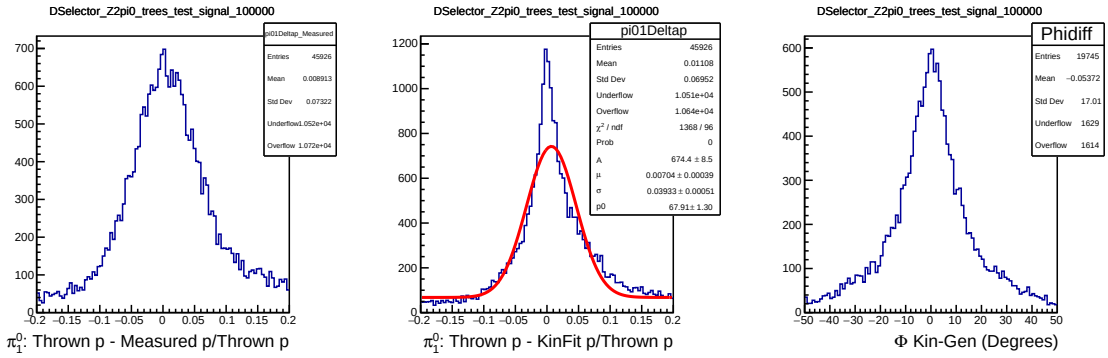

Figure 10: Left: Difference between measured and generated momentum. Center: Difference between kinematically fit and generated momentum. The central peak has a width of about 2%. Right: Difference between the kinematically fit azimuthal angle $\phi_{\pi\pi}$ and its generated value.

in Fig. 11, along with the resolution of Mandelstam $-t$, and the reconstructed time resolution. The mass resolution is about 12 MeV.

4.3 Trigger and acceptance

The Primakoff reaction will transfer all the energy of the beam into four photons, which are going forward. All this energy will be deposited in the FCAL, except for leakage down the beampipe. We expect a simple trigger with an energy threshold in the FCAL should have very high efficiency for any events that can be reconstructed: the FCAL trigger with the total energy threshold around 1 GeV can be used. To estimate trigger rate we used the same method as for TOF trigger rate [22] extracted from the dedicated runs with high random trigger frequency. We used FCAL total energy greater than 1GeV deposited within 40 ns excluding the most inner FCAL layer as a trigger condition. Fig. 12 shows the values for LH2 and "empty" target configurations. Since the proposed lead target is 1.7 times thicker than LH2 target (in rad. lengths), we used "empty" target rate plus the difference between LH2 and "empty" target rates scaled with the factor of 1.7. That gives the value ∼9 kHz for 20 nA beam current.

for this experiment.

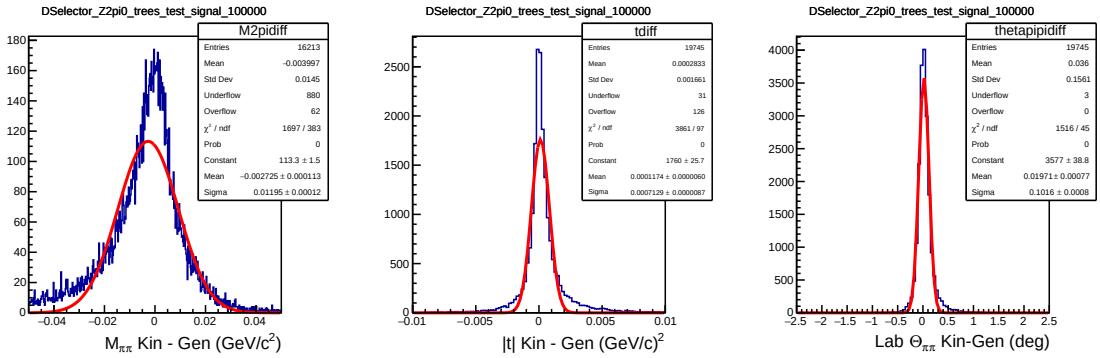

Figure 11: Left: Difference between kinematically fit and generated 2π mass. The central 2π-mass σ is about 12 MeV. Center: Difference between kinematically fit and generated -t. Right: Difference between kinematically fit and generated 2π polar angle. The resolution σ of the reconstructed angle is 0.1 degrees.

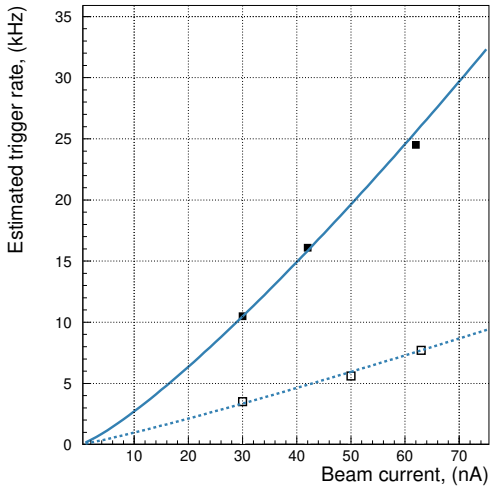

Figure 12: Estimated FCAL trigger rate for 1 GeV total energy threshold for LH2 (solid squares) and "empty" (empty squares) targets.

Table 2: Comparison of backgrounds for the single π^0 channel and the present study for determination of the signal in the $\pi^0\pi^0$ channel. The relative backgrounds for this experiment are expected to be smaller than those for the single π^0 channel.

Integrated Fraction ($\theta < 1.5$ degrees)	$\gamma\, Pb \to \pi^0\, Pb$	$\gamma\, Pb \to \pi^0\pi^0\, Pb$ (This study)
Primakoff signal	1.0	1.0
Nuclear Coherent (NC)	0.39	0.35
Interference	0.12	0.17
$\gamma p \to \eta p$, BR($\eta \to 3\pi^0$)	–	0.37
Incoherent (IC)	0.02	0.06

The acceptance of the signal events can be determined by comparing the kinematically fit to the generated distributions. The generated and kinematically fit 2π mass, $\phi_{\pi\pi}$ and $-t$ distributions are shown in Fig. 13. The reconstruction was described in the previous section. The acceptance is quite high at about 40%. However, there is also significant slewing due to resolution in most variables of interest. The relatively poor resolution in $\phi_{\pi\pi}$ results in dilution of the measured azimuthal dependence, which will need to be adjusted based on simulation. Finally the measured $-t$ resolution roughly reproduces the generated slope despite the smearing of high rate regions down to low rate regions.

5 Backgrounds

We first classify the various backgrounds and then describe each one in more detail. There are two-pion production data on nuclei below 2 GeV [24] in a kinematic regime that is dominated by nucleon resonances. However, at our energy of 6 GeV, the exclusive production of two pions at threshold is very poorly known experimentally, and therefore there are large uncertainties in both the magnitude and the expected distributions of the backgrounds. The major background comes from the $f_0(500)$ 0^+ meson (also referred to as σ-meson in the literature) that decays to two pions. The production mechanism is expected to be very similar to single π^0 0^- production, since the final states are similar except for parity. Therefore, we assume the *relative* background contributions in the single π^0 reaction will be similar in our experiment. The single-pion production distribution on a lead target measured by PrimEx [25] is shown in Fig 14. The relative contributions for π^0 production are plotted in Fig. 15 as a function of angle, highlighting the fact that the Primakoff process is very forward peaked. The integrated fractions are also tabulated for $\theta < 1.5$ degrees in Table 2 and compared to fractions used in this study. Production inside the nucleus will tend to

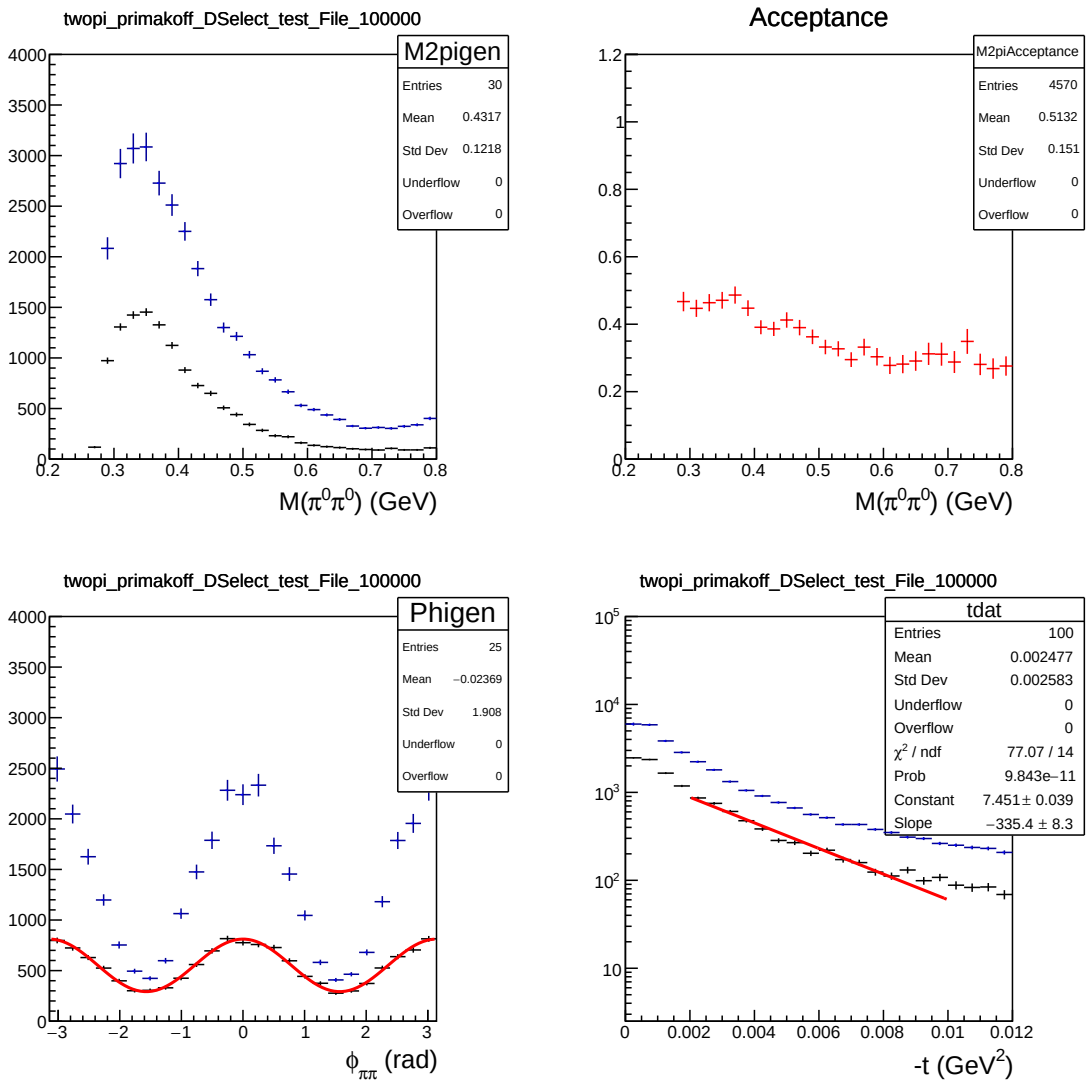

Figure 13: Top left: Generated and kinematically fit (accepted) 2π-mass distribution. Top right: Acceptance as a function of 2π mass. The acceptance is about 40% at threshold. Bottom left: Generated and kinematically fit azimuthal angle $\phi_{\pi\pi}$. Bottom right: Generated and kinematically fit $-t$ distribution.

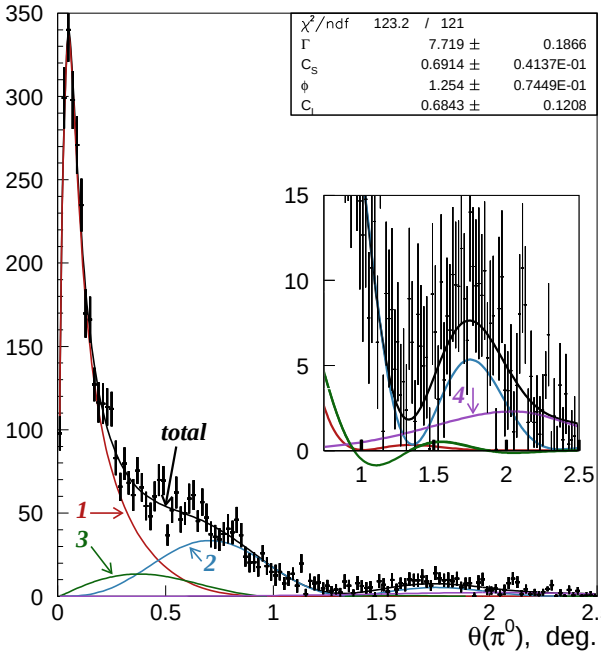

Figure 14: Exclusive π^0 production yield at forward angle on lead target observed in the PrimEx experiment [23]. Curves show the various production mechanisms: 1 – Primakoff, 2 – strong coherent, 3 – interference of first two mechanisms, 4 – strong incoherent

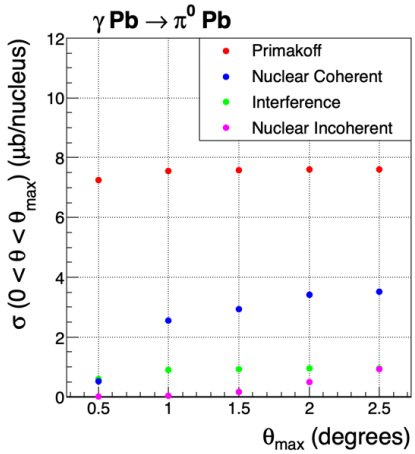

Figure 15: Integrated angular distribution for different contributions to π^0 production in $\gamma\, Pb \to \pi^0\, Pb$ as a function of the upper limit of integration.

reduce hadronic backgrounds in the 2π case due to absorption, but we take a conservative approach and assume that absorption does not change the general picture substantially.

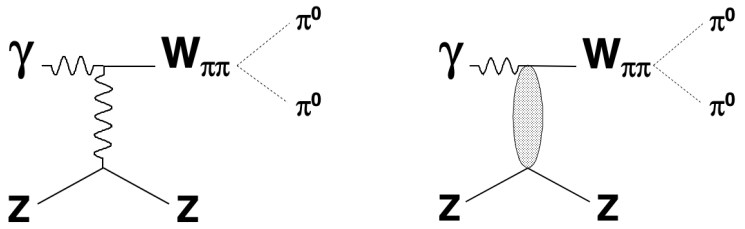

Figure 16: Sketch of coherent two-pion production. Left) Signal: Primakoff mechanism, Right) Backgrounds: Other production mechanisms.

We have the following categories of backgrounds:

- Nuclear coherent production: In this case, the target remains intact. Generically, one may classify the two-pion production according to the sketches in Fig. 16. The left-hand diagram represents the exchange of a virtual photon with the nucleus, i.e., the Primakoff mechanism. This mechanism is very long range, approximately 100 fm, and is affected minimally by the effects of shadowing or absorption. This is the signal for the experiment and our goal is to determine its cross section. The right-hand diagram represents the exchange of a strongly interacting particle (or propagator) and effectively results in the production of pions at the surface of the nucleus. We note that for the $\pi^0\pi^0$ production, pion exchange is not allowed due to charge conjugation conservation, while in the $\pi^+\pi^-$ case, single pion exchange is related to the axial anomaly ($\gamma\pi^0 \to \pi^+\pi^-$). When the interaction leaves the nuclear target intact, the reaction is referred to as "nuclear coherent" and this is one of our most serious backgrounds.

- Incoherent production: When the interaction produces two pions in the quasi-elastic scattering off a single nucleon, the scattered target usually fragments into particles that range out in the target and are unobserved experimentally. This reaction occurs at larger $-t$ and is in general kinematically distinct from the signal. The angular distribution of the $\pi^0\pi^0$ momentum relative to the photon polarization plane is different for Primakoff and incoherent production.

- Any reaction that may be confused with the signal within the experimental resolution or limited acceptance: An example of this type of reaction is Primakoff production of η mesons, where the $\eta \to \pi^0\pi^0\pi^0$ is mis-reconstructed as a two-pion final state.

We note that two important backgrounds for the charged-pion polarizability experiment do not contribute in this experiment: First, coherent ρ^0 photo-production is absent in this experi-

ment because the ρ^0 decay into the $\pi^0\pi^0$ channel is prohibited by Bose statistics. Second, $\mu^+\mu^-$ production is also not a background for an all-neutral final state.

5.1 Nuclear coherent background

The largest coherent backgrounds are from the photoproduction of the $f_0(500)(J^{PC} = 0^{++})$ and the $f_0(980)$. The width of the $f_0(980)$ is fairly narrow and does not contribute directly to the strength near threshold. The $f_0(500)$ width is much broader, from threshold to 800 MeV, with significant overlap in the invariant mass region of interest. Since the $f_0(500)$ is a scalar particle with the same spin-parity as the $\gamma\gamma \to \pi^0\pi^0$ final state near threshold, the azimuthal distribution of the $\pi^0\pi^0$ momentum relative to the photon polarization plane does not differentiate between coherent $f_0(500)$ production and the Primakoff reaction. This is similar to the PrimEx-π^0 experiment, where the dominant background was nuclear coherent π^0 photo-production. The approach used in the PrimEx analysis was to measure the π^0 angular distribution, effectively the t-distribution, then use theoretical calculations of the angular distributions to separate out contributions from Primakoff and nuclear coherent. The analysis of the $\pi^0\pi^0$ (NPP) reaction will follow closely what was done for the PrimEx-π^0 analysis.

We parameterize the $f_0(500)$ meson as detailed in Appendix B and assume that the production amplitude can be factorized as

$$\mathcal{A} \;=\; \mathcal{A}_t(t)\,\mathcal{A}_W(m_{\pi\pi})\,\mathcal{A}_\tau(\Phi,\phi,\theta), \tag{5}$$

where the last factor represents the angular distribution that results in a dependence on the di-pion azimuthal angle, $\phi_{\pi\pi}$, of the form $\mathcal{A}_\tau \propto (1 + \mathcal{P}\cos 2\phi_{\pi\pi})$. The mass dependence is given by the S-wave phase shifts that dominate the mass region below 0.8 GeV. We use the approximate description given in Appendix B.1.[4]

We assume the $-t$ dependence of the $f_0(500)$ has a functional form similar to single π^0 production, namely $\mathcal{A}_t(t) \propto \sin\theta_{\pi\pi} \times F_{st}(t)$. The $\sin\theta_{\pi\pi}$ comes from the spin-flip required at forward angles to produce a 0^+ system off a spin-zero target. The factor $F_{st}(t)$ is the strong form factor for the target, which is approximated to match calculations for the single π^0 production (Fig. 6 from Ref.[26]). Our Gaussian approximation to the form factor is shown in Fig. 17 along side the calculation for single π^0 production. Efforts are underway to calculate the strong form factor for this reaction.[5] The PrimEx data showed that the nuclear coherent process is highly suppressed for heavy nuclei, as shown in Fig.14. The reason for this suppression is π^0 absorption in the nuclear interior, making the coherent production primarily a surface effect. For NPP it is expected that

[4]More detailed studies may require including contributions from the D-wave and S-wave, I=2, amplitudes.
[5]S. Gevorkyan, private communication.

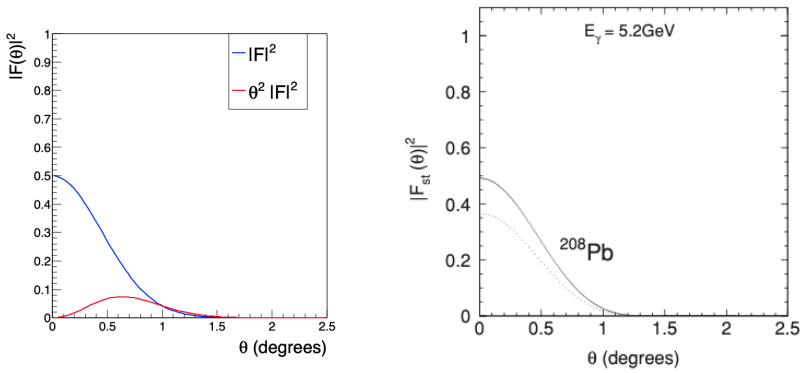

Figure 17: Left) Approximation to strong form factor for lead, Right) Figure 6 from Ref. [26] showing the calculated strong form factor for single π^0 production off a lead target.

suppression of the nuclear coherent process will be approximately twice stronger than that seen in PrimEx because two pions are produced in NPP as compared to a single π^0 in PrimEx.

Fig. 18 shows distributions of interest for a sample of $\pi^0\pi^0$ Primakoff and nuclear coherent background events simulated in approximate proportion to that observed in single pion production. The strong phase between the two production mechanisms is set to 75 degrees for this simulation, where an angle of zero produces maximum interference. This angle must be determined experimentally. The 2π mass and the 2π scattering angle distributions are shown in the top two panels. The Primakoff signal peaks at the 2π-mass threshold and at about 0.2 degrees, whereas the nuclear coherent signal rises linearly from 2π threshold, as expected for $f_0(500)$ production, and peaks at an angle of about 0.8 degrees. The azimuthal angular distribution is the same for both signal and background and has no discriminating power. The angular distributions of the pions in the center of mass of the 2π system are all uniform, and as such do not help in distinguishing the signal from the nuclear coherent background.

5.2 Incoherent two-pion production

In addition to the coherent production of two pions off the nucleus, two pions may also be produced via the elementary reaction $\gamma N \to \pi^0\pi^0 N$, breaking up the nucleus in the process. We model the incoherent background with a mass distribution given by the $f_0(500)$, but with an exponential t dependence given by e^{Bt}, with $B = 3.6$ GeV^{-2}. The slope is taken from Ref.[27] and has very large uncertainties. However, as long as the slope is small compared to Primakoff production, which has an effective slope of $B \sim 560$ GeV^{-2}, it does not change the picture. The mass and angular dependencies are shown in Fig. 19. The strength is small at threshold and at small angles, where

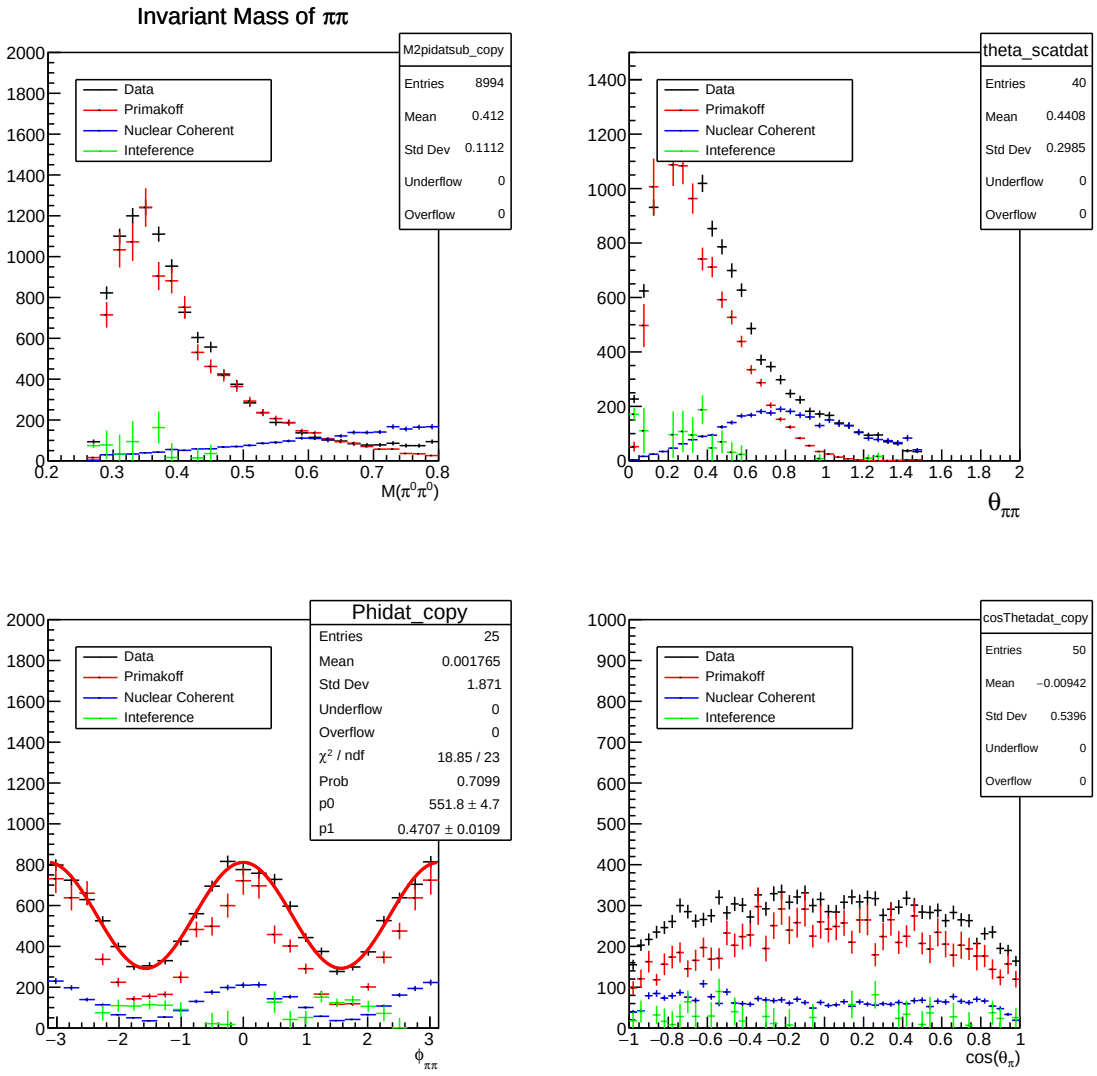

Figure 18: Kinematic distributions for the Primakoff signal and nuclear coherent background only are shown for reference. The MC data (black) are fitted to the sum of the signal and NC background including the interference between amplitudes. Top left) 2π mass, Top right) 2π scattering angle, Bottom left) 2π azimuthal angle, Bottom right) Polar angle of one pion in the 2π center-of-mass.

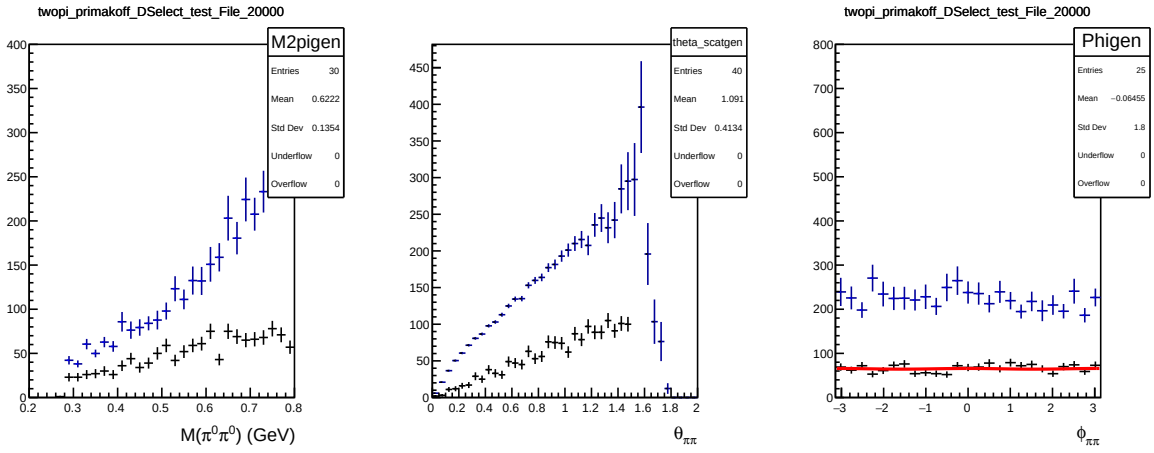

Figure 19: Distributions for the incoherent production off free nucleons. The blue crosses represent the generated distributions and the black crosses represent the kinematically fit accepted distributions. Left) 2π mass. Center) 2π scattering angle. The drop of the generated distribution at 1.5 degrees is due to an analysis cut. Right) 2π azimuthal angle.

Primakoff is strongest. The azimuthal angle is flat, so the photon polarization can also discriminate against this background.

The cross section for this reaction on free protons is relatively large, about 140 nb/nucleon for $0.3 < M_{\pi\pi} < 0.8$ GeV.[6] However, this process is strongly suppressed in nuclei by Pauli blocking and by pion absorption. The Pauli suppression is proportional to $1 - G(t)$, where $G(t)$ is a nuclear form factor and has the limit of $G(t) \to 1$ as $-t \to 0$ [26, 28]. In the case of single π^0 production, incoherent scattering contributes at the level of a couple of percent, and we expect it to be suppressed more strongly in 2π production. See Appendix D for details. Therefore, we expect this background to be about three times smaller than what is used in the present studies.

5.3 Mis-identified backgrounds

There may be important backgrounds that are mistaken for the signal due to mis-identification. These may include

(i) coherent production of η followed by $\eta \to \pi^0\pi^0\pi^0 \to \gamma\gamma\gamma\gamma(\gamma\gamma)$, where only four photons are

[6]The cross section is estimated from the S-wave production of the $f_0(500)$ meson extrapolated to small $-t$ from data archived in the *hepdata.net* database and reported in Ref. [27]. See Appendix B for more information. A factor of one half is applied to the measured cross section for $\pi^+\pi^-$.

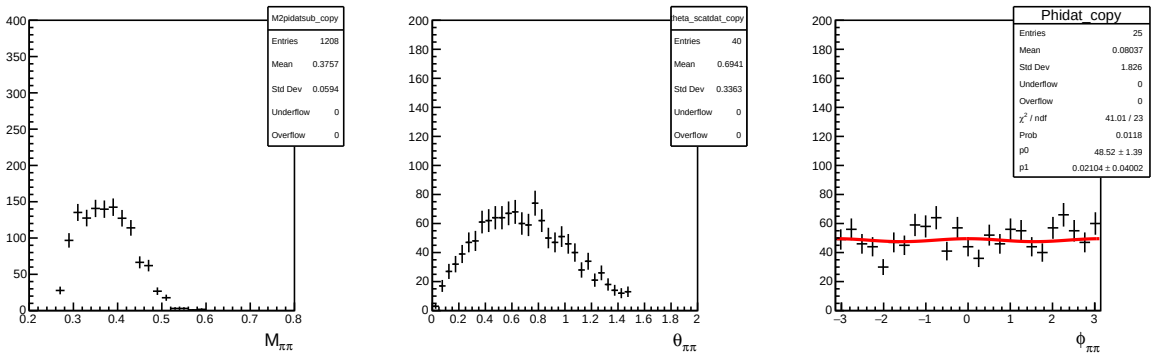

Figure 20: Kinematically fit distributions for η's that decay to $3\pi^0$, but get reconstructed as a $2\pi^0$ final state (broken η's). We generated the sample using the *gen_EtaPb* event generator which simulates the Primakoff mechanism. The distributions produced from the NC mechanism are similar. Left) 2π mass. Center) 2π scattering angle. Right) 2π azimuthal angle.

reconstructed.

(ii) production of nucleon resonances that contribute to the $\gamma N \to N\pi^0\pi^0$ final state. This contribution is expected to be small based on the experience of other Primakoff experiments.

The most important background from mis-identification is due to η production, where the η decays to three π^0s but is reconstructed with a reasonable kinematic fit probability as a $2\pi^0$ final state. We refer to these as "broken" η's. As with π^0 production, η mesons may be produced via the Primakoff process, by the NC process or by quasi-elastic scattering from individual nucleons. The first two mechanisms are the most pernicious, as the incoherent production produces events that fall outside the typical signal kinematics. The incoherent production was investigated using the *genEtaRegge* event generator [29]. As expected, the resulting distributions are very similar to those from incoherent 2π production described in the previous section. If η's are produced via the Primakoff and/or NC mechanisms, they may reconstruct as a 2π final state if one of the decay pions is low energy and goes undetected. The probability for this to happen is at the percent level. We describe these production mechanisms in more detail next.

Two samples of η events were generated, one corresponding to Primakoff-η production and the other due to NC production of η's. These are two-body reactions, so they only differ in the angular distribution of the produced η, or equivalently their t-distribution. In principle these mechanisms interfere, but we generated the samples independent of one another and assumed a uniform azimuthal angular distribution. The events were then processed through the Geant4 Monte

Carlo, which decayed them according to their nominal branching fractions, and then *mcsmear*. These steps were followed by the reaction filter that analyzed the events just as if they were signal, i.e., treated events as $\gamma Pb \to Pb\,\pi^0\pi^0$ with a kinematic fit assuming the recoil target nucleus was missing.

We used a couple of very simple but powerful selection cuts to eliminate the η background. The cuts include a selection on the missing mass squared ($|MM - {M_{Pb}}^2| < 0.1$ GeV^2) and a cut on the $\chi^2 < 5$ of the kinematic fit to $\gamma\, Pb \to \pi^0\pi^0(Pb)$ with a missing recoil. In the analysis we also restrict the 2π scattering angle ($\theta_{\pi\pi} < 1.5$ degrees), which further constrains the range of missing mass. The result of these selections, which have been applied uniformly to signal and background, reduce the contamination from this source to about 37% of the signal. The distributions of the accepted events for the Primakoff-η mechanism are shown in Fig.20. These selections are illustrative and will allow us to achieve our experimental goals but further optimizations may have to be done. We note that the relative number of mis-identified η's in the experiment will be determined empirically from the measured rate of fully reconstructed $\eta \to \pi^0\pi^0\pi^0$ events.

The number of generated Primakoff-η events was determined by using the scaling rules described in Appendix D. The rate of Primakoff-η production was determined relative to Primakoff-π^0 (0.28) and the results in the appendix (Eq. 42) used to determine this rate relative to Primakoff-$\pi^0\pi^0$ (1/0.05), resulting in $\sigma_\eta/\sigma_{\pi^0\pi^0} \sim 6$. We assume that the fraction of NC-η/Primakoff-$\eta \sim 1/3$. The events from each sample were combined in this ratio as backgrounds for use in the study of the extraction of the signal.

6 Extraction of the Primakoff signal

The $\pi^0\pi^0$ Primakoff signal is determined using an amplitude fit[7] to all data simultaneously. It assumes that the mass and angular distributions are known for each of the contributions to the 2π sample. A complex scaling factor is determined for each contribution by doing an unbinned maximum likelihood fit to the event sample. The result of such a fit to the sample that includes the Primakoff and NC processes only, has been shown in Fig. 18. The fit to the MC data that includes the Primakoff-$\pi^0\pi^0$ signal, and backgrounds from NC-$\pi^0\pi^0$, incoherent production and broken η's, is shown in Fig. 21. The generated samples correspond approximately to the expected number of events expected for the experiment. The three kinematic quantities that have the most discriminating power between the signal and background are the 2π mass $M_{\pi\pi}$, the 2π scattering angle $\theta_{\pi\pi}$ and the azimuthal angle $\phi_{\pi\pi}$. The fit uses all the kinematic information contained in the event sample to determine the fraction of signal and background components that are present. A good fit is obtained to the data and the Primakoff signal is determined. The statistical uncertainties as a function of $M_{\pi\pi}$ are obtained directly from the fit (top left plot in Fig. 21). We estimate the

[7] AmpTools, https://github.com/mashephe/AmpTools/wiki.

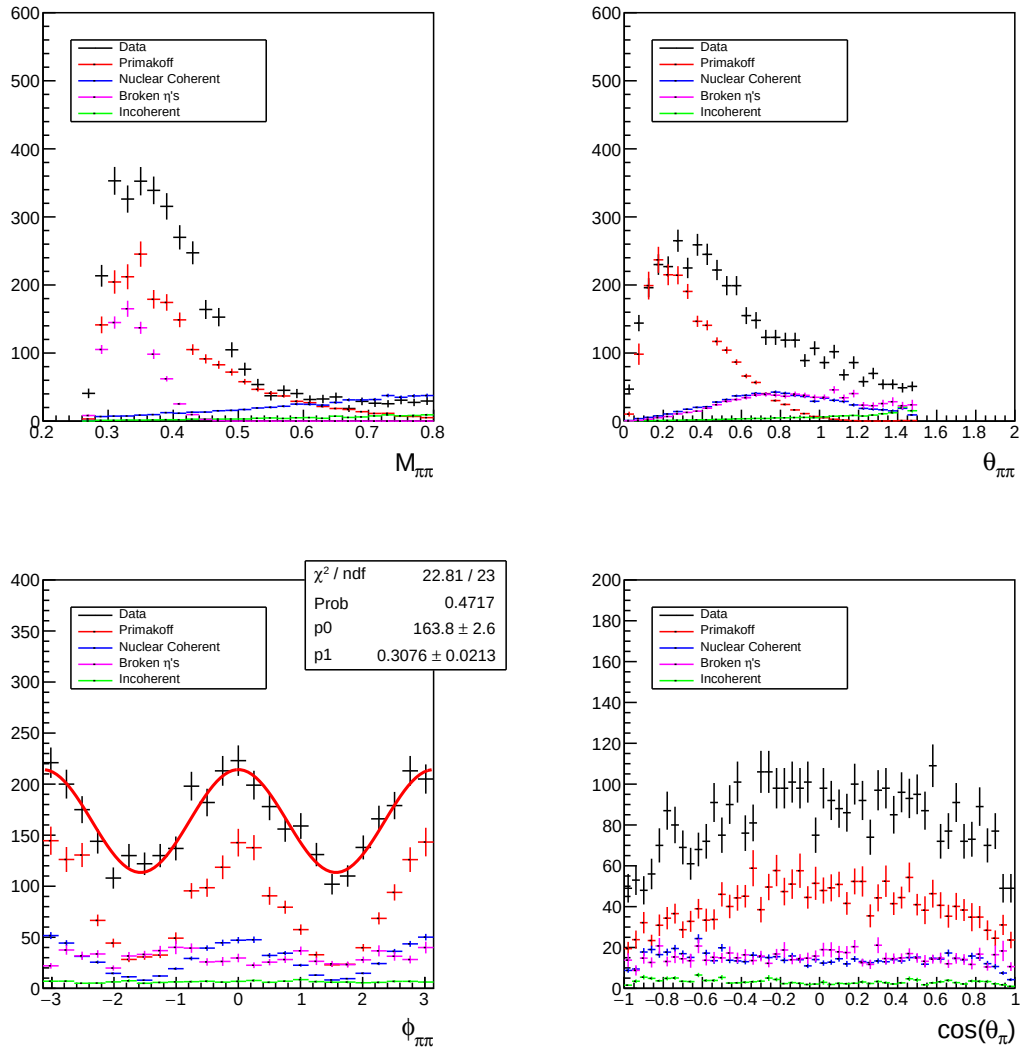

Figure 21: Results of the amplitude fit to the MC data (black points) to extract the amplitudes for the $\pi^0\pi^0$ Primakoff signal, nuclear coherent background, broken η distributions and incoherent background. Top left) 2π mass, Top right) 2π scattering angle, Bottom left) 2π azimuthal angle, Bottom right) Polar angle of one pion in the 2π center-of-mass.

systematic uncertainty (3%) in the extraction of the signal by assuming that the number of broken η's can be known with an uncertainty of 25%.

7 Analysis of existing data

We investigated the challenges of reconstructing $2\pi^0$ final states with a missing recoil proton using the 2017 GlueX data taken with a hydrogen target and the 2019 PrimEx-Eta data with beryllium and helium targets. This is a useful exercise to verify that nearly elastic $2\pi^0$ events can be detected with GlueX and to check the resulting resolutions with real data. Unfortunately, with these targets backgrounds with these targets were too high to be able to extract the Primakoff signal.

7.1 Hydrogen target

We selected and reconstructed events that matched the topology of the reaction $\gamma p \to \gamma\gamma\gamma\gamma\,(p)$ with a missing proton. A kinematic fit was performed that conserved energy and momentum and imposed a vertex constraint at the center of the target cell ($z = 65$ cm). The fit was required to converge. We note that even though the vertex was fixed at 65 cm to perform the fit, the actual target extends from 50 to 80 cm. Several other nominal selection criteria were imposed to clean up the event sample, including the absence of charged tracks and a requirement that there be no missing energy. No constraints were imposed on the π^0 mass to allow study of backgrounds. In addition accidental background subtractions were performed.

The invariant mass distributions of two photon pairs each show a strong π^0 peak, as shown in the top of Fig. 22. There are background events that fall under the two π^0 peaks, which requires further study, nevertheless, using the selection of photon pairs that reconstruct to the π^0, we can plot the $2\pi^0$ mass spectrum (bottom of Fig. 22). The mass spectrum has recognizable features, in particular the prominent $f_2(1270)$ that decays to $\pi^0\pi^0$ 85% of the time. The structure at $M_{\pi\pi}$ ~0.8 GeV appears too low for the $f_0(980)$ and is present in a location where the Crystal Ball data [4] shows a low yield. The yield for $M_{\pi\pi}$ <0.5 GeV is consistent within a factor of two of the relative yield compared to the f_2(1270 peak in the Crystal Ball data. This analysis demonstrates that these neutral events can be analyzed in our detector under significant more challenging circumstances than we anticipate for the Primakoff experiment. In particular, for the Primakoff experiment, we will have a point nuclear target that will allow valid geometrical constraints and limit the amount of missing momentum in the reaction. This will make the kinematic fitting more effective.

It is evident from top plot in fig. 22 that a cut on the invariant mass of one reconstructed π^0 will reduce the background on the other π^0 significantly. This is shown in fig. 23 where a cut on the invariant of one π^0 significantly reduces the background in the other while keeping the main

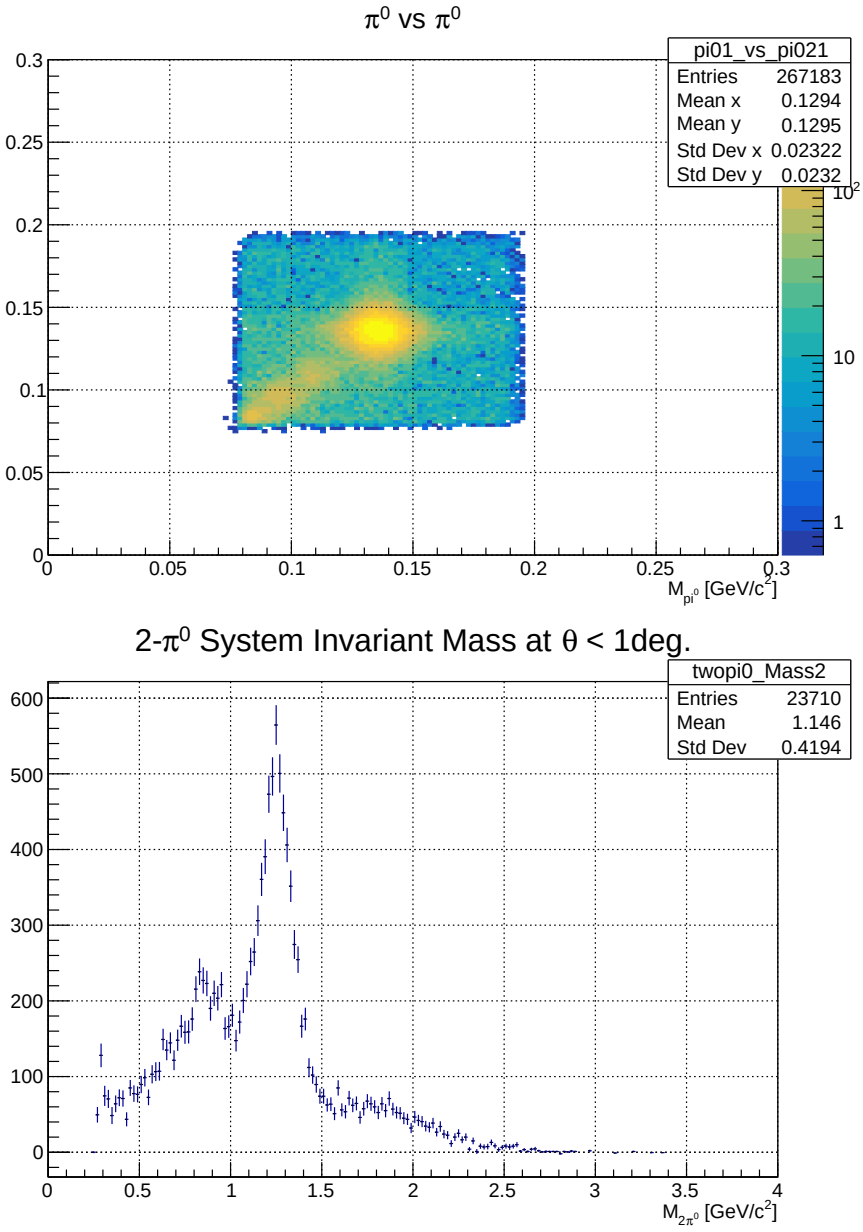

Figure 22: Experimental distributions from the 2017 GlueX data set analyzed as $\gamma p \rightarrow \gamma\gamma\gamma\gamma\,(p)$ with a missing proton. Top: Two photon invariant mass of one pair vs the two photon invariant mass of the second pair. Bottom: 2π mass distribution selecting events with the reconstructed photon pair masses close to the π^0 mass as shown above. The plot also requires that the angle of the two pion system be less than 1 degree.

signal mostly undisturbed.

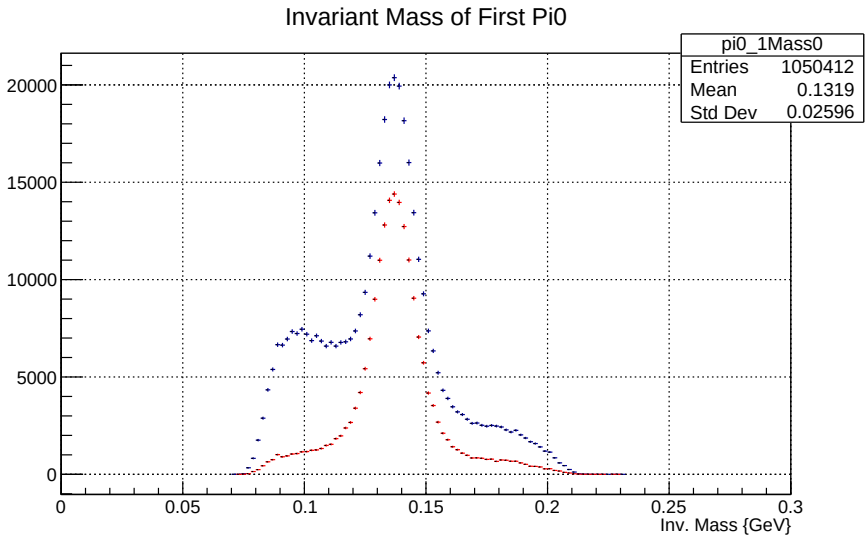

Figure 23: Invariant mass of the two photon system with(red) and without(blue) a cut on the invariant mass of the second pair of photons.

These photons are detected by the lead-glass calorimeter and are the main contribution to the resolution of the reconstructed π^0 mass. A lead-tungstate calorimeter with a substantially better energy resolution would yield a significant improvement in the signal to noise ration as the width of the reconstructed π^0 would be smaller by about a factor of 2.

7.2 Helium and beryllium targets

The PrimEx-Eta experiment collected valuable data on light nuclear targets (^{4}He and ^{9}Be) in 2019. Analysis of the two neutral pion system photoproduction on these nuclei gives a good estimation of the main background sources, signal to background levels, and the Hall-D detector resolution for the main kinematic variables of two neutral pion photoproduction process. The total PrimEx-Eta luminosity corresponds to approximately one day on 5 % rad. len. beryllium target and 18 days on a 4 % rad. len. helium target at 200 nA electron beam current and a 10^{-4} rad. len. thick amorphous tagger radiator. The Beryllium target has a thickness of only 1.5 cm (compare to 30 cm liquid Helium and Hydrogen targets), which allows constraining interaction point (important for the neutral pions reconstruction without any additional vertex information from the tracking system). First we identified the two neutral pion exclusive photoproduction process using the energy ratio of two pions to the initial beam energy with the expected recoil energy subtracted. Fig. 24 shows this distribution for pions detected in FCAL and time accidentals and out-of-target beam interaction

subtracted. We first required exactly four showers to be detected in FCAL and no extra showers

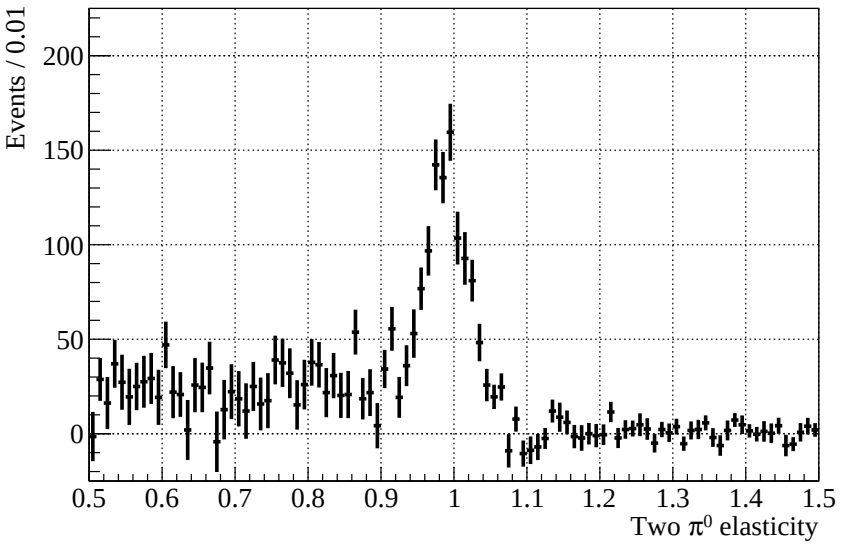

Figure 24: Two neutral pion elasticity (energy ratio to the expected value for the exclusive production) for the Beryllium target.

in BCAL and COMCAL, a minimum shower energy of 0.5 GeV, and no neutral signals in TOF. The number of the signal events here is about 900, the width of the observed signal with pion kinematic fit to the mass is about 3 %, and the signal to background ratio value is promising. Fig. 25 shows two dimensional distribution of those events: elasticity vs invariant mass. One can see the horizontal line of the exclusive production events and vertical line of $K_{short} \to \pi^0\pi^0$ decays, which are separated from each other. Presence of $K_{short} \to \pi^0\pi^0$ decays in the data is really beneficial for the Primakoff analysis since it allows tuning the detector resolution in Monte-Carlo and make an assessment of the level of this value agreement with the data, which is essential for the successful cross-section fitting procedure and systematic uncertainty control.

Including BCAL showers in the neutral pion reconstruction increases the acceptance (especially for large invariant mass region) and number of observed events by an order of magnitude. For the beryllium target this increases the number of exclusive events to ∼10 K and for the helium target to ∼200 K events. Fig. 26 shows two π^0 invariant mass distribution with the energy within 10% of the expected for the exclusive production with BCAL included for low production angle events (below one degree). The f_2 meson peak is clearly seen. Fig. 27 shows elasticity distribution for both helium and beryllium targets with BCAL reconstructions included (time accidentals and "empty" target background subtracted).

To conclude this section, we wish to highlight the good detector resolution for two π^0 pro-

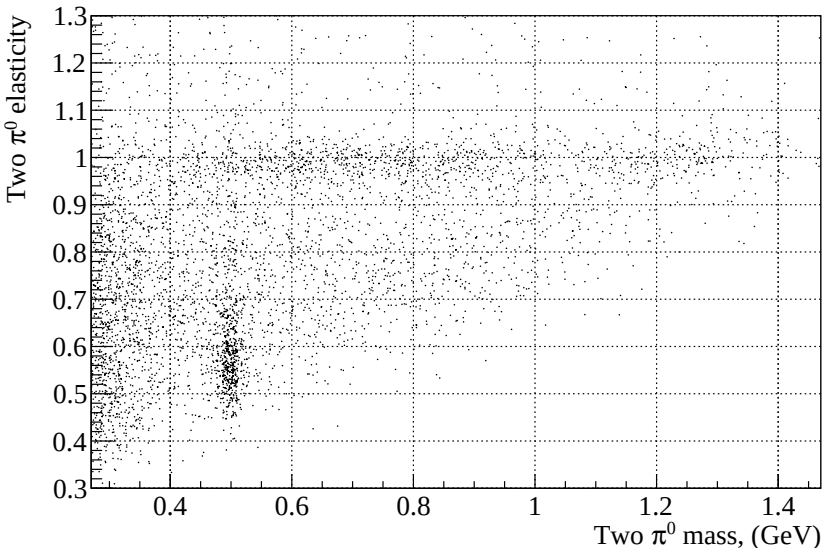

Figure 25: Two neutral pion elasticity (energy ratio to the expected value for the exclusive production) vs invariant mass of two pions for the Beryllium target.

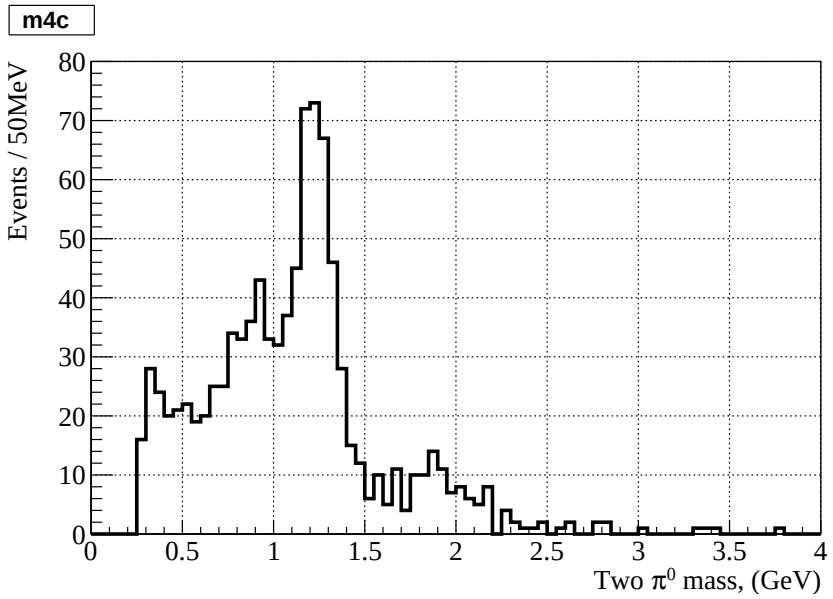

Figure 26: Two neutral pion invariant mass for the exclusive events (within 10% energy), the Beryllium target and production angle below one degree.

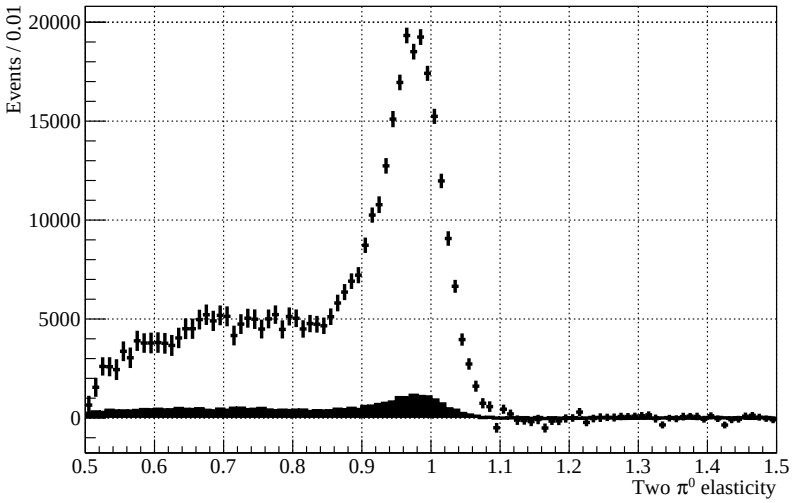

Figure 27: Two pion elasticity distribution with BCAL included in the analysis. "Empty" target and time accidentals are subtracted. Open histogram - Helium target, ∼200 K events in the elastic peak; solid histogram - Beryllium target, ∼10 K events in the peak.

duction kinematics variables, the presence of the calibration process (K_{short}) in the data and controllable level of backgrounds observed for light nuclear targets exposition.

8 Photon beam flux

8.1 Photon beam flux accounting with the GlueX pair spectrometer

The photon beam flux can be directly extracted by analyzing the pair spectrometer (PS) data with the thin beryllium converter installed in the beam in from of it. The absolute normalization of the PS performed with the total absorption counter (TAC) during the dedicated run.

The systematics from the photon beam flux accounting by pair spectrometer is originated from few main contributions: overall spectrometer calibration with TAC quality; accuracy of the Monte-Carlo simulation of this process; long term stability of the spectrometer performance; and change of conditions between low intensity beam (TAC calibration) and production intensity. There are few other less significant contributions. GlueX PS acceptance [30] shown on Fig. 28. For the proposed experiment PS magnetic field should be reduced to cover the beam energy range $5 - 6\,GeV$. The methodology and accuracy of the PS analysis is the same as in PrimEx-D experiment, currently

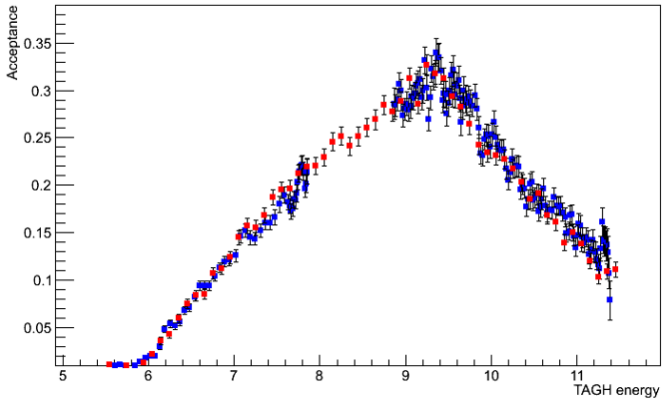

Figure 28: GlueX PS acceptance extracted from TAC data analysis (blue points); red points – Monte-Carlo simulation

running in Hall-D, and has value $\sim 1 - 1.5\,\%$ [31].

8.2 Cross section verification with the exclusive single π^0 photoproduction

The extracted cross section can also be normalized on or independently from PS analysis verified with the π^0 radiative decay width extraction. Fig. 14 shows exclusive single π^0 photoproduction yield at forward angle obtained by the PrimEx experiment and used for π^0 radiative decay width extraction.

The photon beam flux in PrimEx was 0.725×10^{12} for 4.9-5.5 GeV bremsstrahlung spectrum part on 5% rad. len. lead target. The distance between calorimeter and target was $\sim 7.3\,m$ and the central square part of the calorimeter, used in analysis was $\sim 70 \times 70\,cm$. These conditions have to be compared with the proposed experiment conditions: 20 days of 10^7 collimated beam photon/sec (i.e. 20 times more than PrimEx lead target beam flux), the distance between target and FCAL $\sim 6.2\,m$ and active calorimeter part diameter $\sim 2\,m$. The central hole with one calorimeter modules layer around which should be excluded from the analysis for PrimEx case was $\sim 8 \times 8\,cm$ and for FCAL $\sim 20 \times 20\,cm$, which is decreasing FCAL acceptance at forward angle. Comparison of these experimental conditions allows us expecting an order of magnitude higher exclusive single π^0 photoproduction statistics. Thus PrimEx statistical uncertainty for lead will be decreased from $\sim 2.5\,\%$ down to $\sim 1\,\%$. For the systematical uncertainty, in PrimEx it was $\sim 2.1\,\%$ and has two major contributions: yield extraction ($\sim 1.6\,\%$) and photon beam flux accounting ($\sim 1.0\,\%$). The

first contribution is partly statistically driven and reduces with increasing of statistics; and the second one cancels out since it is the same photon beam flux for the single and double exclusive π^0 photoproduction. The main factors increasing systematics for the proposed experiment are: the angular resolution of FCAL is about a factor of two worse than for PWO crystals used in the PrimEx analysis; and the magnetic field is not swiping out charged background like it was in PrimEx. As a result we can expect slightly worse systematical uncertainty than in PrimEx and statistical precision of $\sim 1\,\%$, i.e. total error $2.5 - 3.5\,\%$ for π^0 radiative width extraction (excluding absolute photon beam flux accounting, target number of atoms and partly FCAL trigger efficiency contributions to the systematics which are canceling out). The expected total beam flux uncertainty for such a normalization should also include the PrimEx total error of the π^0 radiative width, which was recently reported as 1.5% [25]. All this gives $\sim 3 - 4\,\%$ error for photon beam flux from normalization to the re-extracted π^0 radiative decay width.

8.3 Muon pair production

In addition to these normalization channels, production of muon pairs, which has a known cross section, can be used as a measurement of photon flux. Since the experiment will be running concurrently with the Charged Pion Polarizability (CPP) experiment, the photon flux on target will be the same by definition. CPP plans to use muon pair creation by beam photons as its main normalization channel, and so those measurements will be available for normalization of the neutral pion channel as well. In the case of CPP, the GlueX track finding and fitting efficiency will have to be determined for muon pairs, but any systematic error in that determination will largely cancel when applied to charged pion pairs. That will not be the case for the neutral pion channel and will have to be taken into account when evaluating systematic errors due to this method of normalization. In any case, muon pair production should provide a useful check on the other methods mentioned above.

9 Errors and sensitivity

We summarize the anticipated errors in the determination of the π^0 polarizability. We assume 20 days of running on a 5% radiation length ^{208}Pb target, 10^7 photons/s, and nominal acceptance for $\pi^0\pi^0$. Table 3 summarizes the estimated statistical and systematic errors. In the following we describe each of these contributions in detail:

1. Statistical uncertainty in extraction of the Primakoff signal as determined by the fit shown in the top left plot in Fig. 21 (Section 6).

2. Systematic uncertainty in extraction of the signal. This contribution is estimated to be 3%

Table 3: Uncertainties in the extraction of π^0 polarizabilities $\alpha_{\pi^0} - \beta_{\pi^0}$.

	Source	Uncertainty
1	Statistical uncertainty	2.3 %
2	Signal extraction	3.0 %
3	Detector acceptance and efficiency	3.5 %
4	Total systematic error	4.6%
5	Total error on cross section	5.1%
6	Projected error in $\alpha - \beta$	39%

based on differences obtained in the Primakoff signal by varying the amount of background contributions (Section 6).

3. Detector acceptance and efficiency. We measure the cross section for two-pion production relative to single-pion production (Section 8.2). The flux factors cancel. Remaining is the uncertainty in the detector acceptance times efficiency for $\gamma\mathrm{Pb} \to \pi^0\pi^0\mathrm{Pb}$ relative to $\gamma\mathrm{Pb} \to \pi^0\mathrm{Pb}$, which we estimate to be 3.5%.

4. Total systematic error (items 2-3): combining the systematic errors in quadrature gives 4.6%.

5. Error on cross section (quadrature sum of items 1 and 4): 5.1%.

6. The current estimate by Dai and Pennington (Table II in Ref. [17]) indicates that a 13% determination of $\sigma(\gamma\gamma \to \pi^0\pi^0)$ will determine the combination $\alpha_{\pi^0} - \beta_{\pi^0}$ to a precision of 100%, i.e., $\Delta(\alpha_{\pi^0} - \beta_{\pi^0}) \sim 7.7\Delta(\sigma)$. From here we estimate that our uncertainty on $\Delta(\alpha_{\pi^0} - \beta_{\pi^0}) \sim 39\%$. We note that the basis for extracting the polarizabilities may be improved in the near future and theoretical effort is being directed specifically toward this goal.

10 Summary and beam request

We have investigated the possibility of determining the neutral pion polarizabilities $\alpha_{\pi^0} - \beta_{\pi^0}$, a quantity for which there are no existing measurements. Our proposal is to extract the polarizability from a measurement of the cross section of the Primakoff reaction $\gamma\mathrm{Pb} \to \pi^0\pi^0\mathrm{Pb}$. We propose to make this measurement using data taken simultaneously with the CPP[1] experiment in Hall D. Table 4 summarizes the approved beam request for the CPP experiment. The existing GlueX detector has sufficient resolution and high acceptance for this process. We expect to collect

Table 4: Approved beam request and running conditions for CPP. NPP would run concurrently.

Running condition	
Days for production running	20
Days for calibrations	5
Target	^{208}Pb
Photon intensity in coherent peak	10^7 photons/s
Edge of coherent peak	6 GeV

approximately 1800 signal events during the approved 20 PAC days. The anticipated uncertainties on the signal represent a significant improvement over existing data as shown in Fig. 29. Using the estimate by Dai and Pennington [17] we expect to be able to make the first extraction of the $\alpha_{\pi^0} - \beta_{\pi^0}$ polarizability with an uncertainty of 39%.

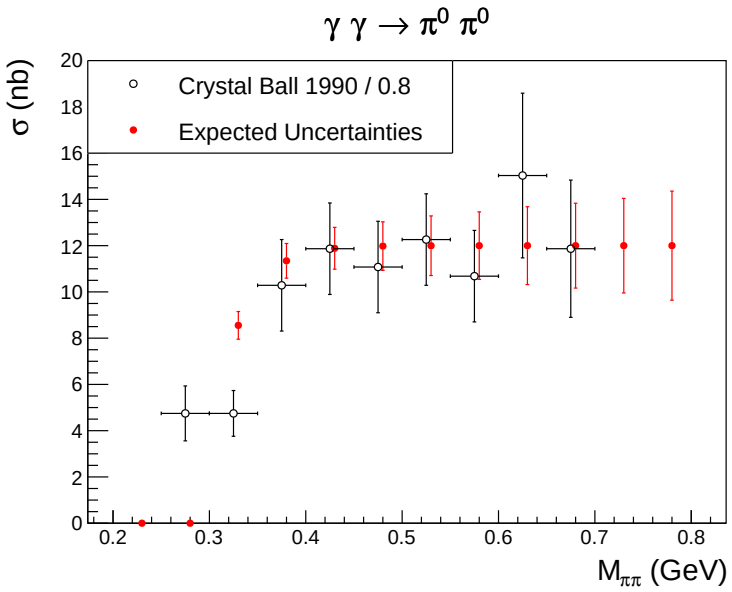

Figure 29: Estimated uncertainties (systematic and statistical errors are added in quadrature) in determining $\sigma(\gamma\gamma \to \pi^0\pi^0)$ during 20 PAC days running simultaneously with the approved CPP experiment. The data points from the single previous Cristal Ball measurement [4] are shown for comparison.

References

[1] JLAB Experiment E12-13-008. Measuring the Charged Pion Polarizability in the $\gamma\gamma \to \pi^+\pi^-$ Reaction, 2013. `https://misportal.jlab.org/mis/physics/experiments/viewProposal.cfm?paperId=789`.

[2] Barry R. Holstein. Pion polarizability and chiral symmetry. *Comments Nucl. Part. Phys.*, 19(5):221–238, 1990.

[3] M. Tanabashi et al. Review of Particle Physics. *Phys. Rev.*, D98(3):030001, 2018.

[4] H. Marsiske et al. A Measurement of $\pi^0\pi^0$ Production in Two Photon Collisions. *Phys. Rev.*, D41:3324, 1990.

[5] S. Bellucci, J. Gasser, and M. E. Sainio. Low-energy photon-photon collisions to two loop order. *Nucl. Phys.*, B423:80–122, 1994. [Erratum: Nucl. Phys.B431,413(1994)].

[6] Juerg Gasser, Mikhail A. Ivanov, and Mikko E. Sainio. Low-energy photon-photon collisions to two loops revisited. *Nucl. Phys.*, ib728:31–54, 2005.

[7] A. Aleksejevs and S. Barkanova. Electromagnetic Polarizabilities of Mesons. *Nucl. Part. Phys. Proc.*, 273-275:2773–2776, 2016.

[8] J. A. Oller and L. Roca. Two photons into pi0 pi0. *Eur. Phys. J.*, A37:15–32, 2008.

[9] Ling-Yun Dai and Michael R. Pennington. Comprehensive amplitude analysis of $\gamma\gamma \to \pi^+\pi^-, \pi^0\pi^0$ and $\overline{K}K$ below 1.5 GeV. *Phys. Rev.*, D90(3):036004, 2014.

[10] Ling-Yun Dai and M. R. Pennington. Two photon couplings of the lightest isoscalars from BELLE data. *Phys. Lett.*, B736:11–15, 2014.

[11] B. Moussallam. Unified dispersive approach to real and virtual photon-photon scattering at low energy. *Eur. Phys. J.*, C73:2539, 2013.

[12] J. Gasser and H. Leutwyler. Chiral Perturbation Theory to One Loop. *Annals Phys.*, 158:142, 1984.

[13] M. Bychkov et al. New Precise Measurement of the Pion Weak Form Factors in $\pi^+ \to e^+\nu\gamma$ Decay. *Phys. Rev. Lett.*, 103:051802, 2009.

[14] S. Bellucci. Pion (kaon) and sigma polarizabilities. In *Chiral dynamics: Theory and experiment. Proceedings, Workshop, Cambridge, USA, July 25-29, 1994*, pages 177–189, 1994.

[15] John F. Donoghue and Barry R. Holstein. Photon-photon scattering, pion polarizability and chiral symmetry. *Phys. Rev.*, D48:137–146, 1993.

[16] Jose A. Oller, Luis Roca, and Carlos Schat. Improved dispersion relations for gamma gamma —¿ pi0 pi0. *Phys. Lett.*, B659:201–208, 2008.

[17] Ling-Yun Dai and Michael R. Pennington. Pion polarizabilities from $\gamma\gamma \to \pi\pi$ analysis. *Phys. Rev.*, D94(11):116021, 2016.

[18] T. Mori et al. High statistics measurement of the cross-sections of $\gamma\gamma \to \pi^+\pi^-$*production*. *J. Phys. Soc. Jap.*, 76:074102, 2007.

[19] S. Uehara et al. High-statistics measurement of neutral pion-pair production in two-photon collisions. *Phys. Rev.*, D78:052004, 2008.

[20] S. Uehara et al. High-statistics study of neutral-pion pair production in two-photon collisions. *Phys. Rev.*, D79:052009, 2009.

[21] E.S. Smith. Calculation of the Primakoff cross section for $\pi^+\pi^-$. Technical Report GlueX-doc-**3186**, Jefferson Lab, January 2017. `https://halldweb.jlab.org/doc-private/DocDB/ShowDocument?docid=3186`.

[22] I. Larin et al. TOF trigger rate study with lead shielding. Technical Report GlueX-doc-**4065**, 2019. `https://halldweb.jlab.org/doc-private/DocDB/ShowDocument?docid=4065`.

[23] I. Larin et al. A New Measurement of the π^0 Radiative Decay Width. *Phys. Rev. Lett.*, 106:162303, 2011.

[24] S. Schadmand. Double Pion Photoproduction from Nuclei, 2005. arXiv:nucl-ex/0504012.

[25] I. Larin. $\pi^0 \to \gamma\,\gamma$ Decay width: Final result from the PrimEx Collaboration, Oct 2018. DNP Meeting.

[26] S. Gevorkyan, A. Gasparian, L. Gan, I. Larin, and M. Khandaker. Photoproduction of Pseudoscalar Mesons off Nuclei at Forward Angles. *Phys. Rev.*, C80:055201, 2009.

[27] M. Battaglieri et al. Photoproduction of pi+ pi- meson pairs on the proton. *Phys. Rev.*, D80:072005, 2009.

[28] S. Gevorkyan et al. Technical Report PRIMEX note, Joint Institute for Nuclear Research, Dubna, August. `https://www.jlab.org/primex/primex_notes/inc.pdf`.

[29] S. Taylor. Modeling the η and η' cross sections. Technical Report GlueX-doc-**2437**, Jefferson Lab, February 2014. `https://halldweb.jlab.org/doc-private/DocDB/ShowDocument?docid=2437`.

[30] A. Somov. Status of the Beam Flux Normalization from TAC runs. Technical Report GlueX-doc-**3684**, Jefferson Lab, February 2018. `https://halldweb.jlab.org/doc-private/DocDB/ShowDocument?docid=3684`.

[31] JLAB Experiment E12-10-011. A Precision Measurement of the eta Radiative decay Width via the Primakoff Effect, 2010. https://misportal.jlab.org/mis/physics/experiments/viewProposal.cfm?paperId=631.

[32] S.U. Chung. Spin Formalisms – Updated Version, Appendix B. Technical Report BNL-QGS-**02-0900**/CERN 71-8, Brookhaven National Laboratory, July 2014. http://suchung.web.cern.ch/suchung/.

[33] J. R. Pelaez. From controversy to precision on the sigma meson: a review on the status of the non-ordinary $f_0(500)$ resonance. *Phys. Rept.*, 658:1, 2016.

[34] L Bibrzycki et al. Meson resonances in forward-angle $\pi^+\pi^-$ photoproduction, 2018. arXiv:1809.06123.

[35] I. J. R. Aitchison and M. G. Bowler. Rescattering Effects in the Deck Model. *J. Phys.*, G3:1503, 1977.

[36] B. Ananthanarayan, G. Colangelo, J. Gasser, and H. Leutwyler. Roy equation analysis of pi pi scattering. *Phys. Rept.*, 353:207–279, 2001.

[37] K. Schilling, P. Seyboth, and Guenter E. Wolf. On the Analysis of Vector Meson Production by Polarized Photons. *Nucl. Phys.*, B15:397–412, 1970. [Erratum: Nucl. Phys.B18,332(1970)].

[38] Carlos W. Salgado and Dennis P. Weygand. On the Partial-Wave Analysis of Mesonic Resonances Decaying to Multiparticle Final States Produced by Polarized Photons. *Phys. Rept.*, 537:1–58, 2014.

[39] M. Jacob and G. C. Wick. On the general theory of collisions for particles with spin. *Annals Phys.*, 7:404–428, 1959. [Annals Phys.281,774(2000)].

[40] E. Leader. *Spin in Particle Physics*. Cambridge University Press, The Edinburgh Building, Cambridge CB2 2RU, UK, 2005.

[41] R. L. Anderson et al. High-energy π^0 photoproduction from hydrogen with unpolarized and linearly polarized photons. *Phys. Rev.*, D4:1937, 1971.

A More on theoretical predictions

The scattering amplitude for $\gamma\gamma^* \to \pi^0\pi^0$ is given in terms of the Compton tensor, whose low energy expansion in the Compton scattering channel $\gamma\pi^0 \to \gamma\pi^0$ is given in terms of the electric and magnetic polarizabilities of the π^0. For the case of interest with one real photon, the Compton tensor is given in by two amplitudes, namely:

$$\begin{aligned} T_{\mu\nu} &= -(A(s,t,u) + \frac{1}{4}B(s,t,u))(\frac{1}{2}\, s\, g_{\mu\nu} - k_\nu q_\mu) \quad (6) \\ &+ \frac{1}{4s}B(s,t,u)((s-q^2)p_{-\mu}p_{-\nu} - 2(k\cdot p_-\ q_\mu p_{-\nu} + q\cdot p_- k_\nu p_{-\mu} - g_{\mu\nu}k\cdot p_-\ \ q\cdot p_-) \quad (7) \end{aligned}$$

Here $s = W^2_{\pi\pi}$ is the invariant mass squared of the two π^0s, k the momentum of the beam photon, q the momentum of the virtual photon, and p_- the $p_- = p_1 - p_2$ the momentum difference between the two pions.

The limit of interest for the polarizabilities is:

$$\begin{aligned} \alpha_\pi &= -\frac{\alpha}{2M_\pi}(A(s,t,u) - \frac{2}{s}M_\pi^2 B(s,t,u))|_{s=0,t=u=M_\pi^2} \\ \beta_\pi &= \frac{\alpha}{2M_\pi}A|_{s=0,t=u=M_\pi^2} \end{aligned} \quad (8)$$

where α_π β_π are the electric and magnetic polarizabilities respectively.

The low energy limit is analyzed in ChPT. At the lowest significant order, i.e., one loop, the π^0 polarizabilities are entirely given in terms of known quantities, namely:

$$\alpha_{\pi_0} = -\beta_{\pi_0} = -\frac{\alpha}{96\pi^2 M_\pi F_\pi^2} \simeq -0.55 \times 10^{-4}\ \text{fm}^3 \quad (9)$$

The positive magnetic susceptibility indicates that the π_0 is diamagnetic, and naturally the negative electric polarizability tells that it behaves as a dielectric.

There are higher order corrections in the chiral expansion to the above prediction corresponding to a two-loop calculation, which is undefined up to two low energy constants $h_\pm$ in the notation of Ref. [5], expected to be significant for the corrections.

The amplitudes A and B are constrained by unitarity and analiticity to satisfy dispersion relations. In particular below $s \sim 0.8$ GeV^2 the dominant contributions are for the pair of pions in an S-wave. The rather well established S-wave phase shifts thus allow for implementing dispersion relations [15, 8, 11, 9, 10, 17]. In this proposal the model by Donoghue and Holstein [15] for implementing the dispersive representation using S-wave final state interaction was adopted. The model implements twice subtracted dispersion relations for the isospin 0 and 2 components of the

amplitude A with the addition of t- and u-channel resonance exchanges for both A and B. The four subtraction constants require the experimental input of the cross section to be measured by the proposed experiment.

A summary of useful theory results is the following:

1) representation of the Compton amplitudes:

$$\begin{aligned} s\,A(s,t,u) &= -\frac{2}{3}(f_0(s)-f_2(s))+\frac{2}{3}(p_0(s)-p_2(s))-\frac{s}{2}\sum_{V=\rho,\omega}R_V(\frac{t+M_\pi^2}{t-M_V^2}+\frac{u+M_\pi^2}{u-M_V^2}) \\ B(s,t,u) &= -\frac{1}{8}\sum_{V=\rho,\omega}R_V(\frac{1}{t-M_V^2}+\frac{1}{u-M_V^2}) \\ R_V &= \frac{6M_V^2}{\alpha}\frac{\Gamma(V\to\pi\gamma)}{(M_V^2-M_\pi^2)^3} \end{aligned} \tag{10}$$

where $V=\rho,\ \omega$,

$$\begin{aligned} p_I(s) &= f_I^{\rm Born}(s)+p_I^A(s)+p_I^\rho(s)+p_I^\omega(s) \\ p_0^A(s)=p_2^A(s) &= \frac{L_9^r+L_{10}^r}{F_\pi^2}\left(s+\frac{M_A^2-M_\pi^2}{\beta(s)}\log\frac{1+\beta(s)+s_A/s}{1-\beta(s)+s_A/s}\right) \\ p_0^\rho(s) &= \frac{3}{2}R_\rho\left(\frac{M_\rho^2}{\beta(s)}\log\frac{1+\beta(s)+s_\rho/s}{1-\beta(s)+s_\rho/s}\right) \\ p_2^\rho(s) &= 0 \\ p_0^\omega(s)=-\frac{1}{2}p_0^\omega(s) &= -\frac{1}{2}R_\omega\left(\frac{M_\omega^2}{\beta(s)}\log\frac{1+\beta(s)+s_\omega/s}{1-\beta(s)+s_\omega/s}-s\right), \end{aligned} \tag{11}$$

where $\beta(s)=\sqrt{\frac{s-4M_\pi^2}{s}}$, M_A the mass of the A_1 resonance. The f_Is are given by the dispersive representation:

$$f_I(s) = p_I(s)+\Omega_I(s)\left(c_I+d_I\,s-\frac{s^2}{\pi}\int_{4M_\pi^2}^\infty p_I(s')\mathrm{Im}(\Omega_I^{-1}(s'))\frac{ds'}{(s'-s)s'^2}\right), \tag{12}$$

with the Omnès function:

$$\Omega_I(s>4M_\pi^2) = e^{i\phi_I(s)}\exp\left(\frac{s}{\pi}\int_{4M_\pi^2}^\infty\frac{\phi_I(s')-\phi_I(s)}{s'-s}\frac{ds'}{s'}+\frac{\phi_I(s)}{\pi}\log\frac{4M_\pi^2}{s-4M_\pi^2}\right). \tag{13}$$

the phases ϕ_I are related to the corresponding $\pi\pi$ S-wave phase shifts according to:

$$\begin{aligned} \phi_0(s) &= \theta(M-\sqrt{s})\delta_0^0(s)+\theta(\sqrt{s}-M)(\pi-\delta_0^0(s)) \\ \phi_2(s) &= \delta_0^2(s), \end{aligned} \tag{14}$$

where M is the mass of the f_0 resonance.

The values used for the parameters entering the representations above are:

$$\begin{aligned} L_9^r + L_{10}^r &= 1.43 \pm 0.27 \times 10^{-3} \\ s_i &= 2(M_i^2 - M_\pi^2) \\ R_\omega &= 1.35/\text{GeV}^2; \quad R_\rho = 0.12/\text{GeV}^2 \end{aligned} \tag{15}$$

and the $\pi\pi$ phase shifts are well approximated up to $\sqrt{s} \sim 1.5$ GeV by the parametrization:

$$\delta_0^I(s) = \arcsin\left(\frac{\Gamma_I}{2\sqrt{(\sqrt{s} - M_I)^2 + \frac{\Gamma_I^2}{4}}}\right) + \sum_{n=0}^{N} a_n \ (\sqrt{s})^n \tag{16}$$

where we include one single resonance for each $I = 0, 2$.

For the available data we need only up to $N = 3$ for $I = 0$, with the result:

$$\begin{aligned} M_0 = 0.994 \text{ GeV}; &\qquad \Gamma_0 = 0.0624 \text{ GeV} \\ a_0 = -1.439; &\qquad a_1 = 6.461/\text{GeV}; \quad a_2 = -5.529/\text{GeV}^2; \quad a_3 = 2.022/\text{GeV}^3 \end{aligned} \tag{17}$$

For the case $I = 2$ one finds that the resonance term is not needed at all and a good fit is provided with $N = 3$ with the result:

$$a_0 = -0.878; \qquad a_1 = -0.611/\text{GeV}; \quad a_2 = -0.083/\text{GeV}^2; \quad a_3 = 0.115/\text{GeV}^3 \tag{18}$$

The $\gamma\gamma \to \pi_0\pi_0$ in the S-wave approximation valid up to about $\sqrt{s} \sim 0.9$ GeV is given by:

$$\begin{aligned} \sigma_{\gamma\gamma\to\pi^0\pi^0}(|\cos\theta| < Z)(s) &= \frac{\pi\alpha_{EM}^2}{s^2}\frac{Z}{2}\sqrt{s(s-4M_\pi^2)} \\ &\times \ (\mid A(s)s - M_\pi^2 B(s) \mid^2 \\ &+ \ \frac{1}{s^2}\left(M_\pi^4 - \frac{1}{16}(\frac{Z^2}{3}s(4M_\pi^2 - s) + 4(s - 2M_\pi^2)^2)\right) \mid B(s) \mid^2) \end{aligned} \tag{19}$$

Fitting to the Cristal Ball data[4] the parameters $c_0,\ d_0,\ c_2,\ d_2$ can be estimated, giving in the corresponding units:

$$\begin{aligned} c_0 &= -0.529 \\ d_0 &= -2.033 \\ c_2 &= 0.953 \\ d_2 &= -1.271. \end{aligned} \tag{20}$$

B Parameterization of the nuclear coherent production

We consider the reaction $\gamma A \to m_{\pi\pi} A$, where $m_{\pi\pi} \to \pi\pi$ is a dipion system. The 2π system is treated as a particle with mass $m_{\pi\pi}$, which is produced with four-momentum transfer t. The cross section for a three-body final state can be written as [32]:

$$
\begin{aligned}
d\sigma &= \frac{1}{4\mathcal{F}}\, d\phi_3\, |\mathcal{A}|^2 && (21)\\
\mathcal{F} &= p_\gamma^{cm}\sqrt{s} && (22)\\
d\phi_3 &= \frac{4}{(4\pi)^5}\frac{p_\sigma^{cm}}{\sqrt{s}} d\Omega_\sigma^{cm}\, p_\pi^\sigma dm_{\pi\pi} d\Omega_\pi^\sigma && (23)\\
\frac{dt}{d\Omega_\sigma^{cm}} &= \frac{dt}{d\cos\theta_\sigma^{cm} d\phi_\sigma^{cm}} = \frac{2\, p_\gamma^{cm} p_\sigma^{cm}}{d\phi_\sigma^{cm}} && (24)
\end{aligned}
$$

The center-of-mass energy (cm) energy and the momentum transfer are represented by the commonly used variables s and t. Other variables are subscripted by particle name and their superscripts indicate the reference frame. Thus p_γ^{cm} is the incident photon momentum, p_σ^{cm} is the scattered momentum, and Ω_σ^{cm} corresponds to the solid angle of the σ, all in the cm frame. The momentum of the pions in the σ rest frame is denoted by p_π^σ and Ω_π^σ denotes the solid angle of one of them. Thus the cross section can be written as

$$
\frac{d\sigma}{dt dm_{\pi\pi} d\phi_\sigma^{cm} d\Omega_\pi^\sigma} = \frac{1}{2(4\pi)^5}\frac{p_\pi^\sigma}{(p_\gamma^{cm})^2 s}\Big|\sum_i \mathcal{A}^i\Big|^2, \qquad (25)
$$

where the index i runs over the number of resonances or mechanisms included in the calculation. We will assume that we can parameterize each production amplitude as a factorized product

$$
\mathcal{A}^i = \mathcal{A}_t(t)^i\, \mathcal{A}_W(m_{\pi\pi})^i\, \mathcal{A}_\tau(\Phi,\phi,\theta)^i. \qquad (26)
$$

For simplicity, we will drop the superscript i since for the moment we are considering single production mechanism. The function $\mathcal{A}_\tau(\phi_{\pi\pi},\phi_\pi,\theta_\pi)$ contains the angular dependence of the produced pions, where (θ_π,ϕ_π) are the decay angles in the rest frame of the 2π system, which is flat for S-wave production. Azimuthal symmetry is broken by the photon polarization, where $\phi_{\pi\pi}$ is the angle between the plane of photon polarization and the production plane. The amplitudes are given by Eq. 41 and lead to a cross section dependence of the form $\mathcal{A}_\tau \propto (1+\mathcal{P}\cos 2\phi_{\pi\pi})$.

The primary background in this mass region is given by the $f_0(500)(J^{PC}=0^{++})$ also called the σ. The σ has the same angular structure as the Primakoff reaction and can only be identified through its dependence on t and $m_{\pi\pi}$. Our parameterization of the mass dependence for the σ meson is described in Section B.1.

We assume the $-t$ dependence of the σ has a similar form as for single π^0 production, namely $\mathcal{A}_t(t) \propto \sin\theta_{\pi\pi} \times F_{st}(t)$. The $\sin\theta_{\pi\pi}$ comes from the spin-flip required at forward angles to produce a 0^+ system from a spin-zero target. The factor $F_{st}(t)$ is the strong form factor for the target, which is approximated to match calculations for the single π^0 production (Fig. 6 from Ref.[26]).

B.1 Parameterization of the s-wave amplitude

There is considerable strength in the 2π channel coming from s-wave production, which is due to the now established $f_0(500)$ meson. It is also commonly referred to as the σ meson. We assume the amplitude for σ production is governed by the $\pi\pi$ J=0, I=0 phase shifts. We parameterize the $m_{\pi\pi}$ dependence as

$$\mathcal{A}_W(m_{\pi\pi}) \;\sim\; \frac{m_{\pi\pi}}{2k}\sin\delta_0 e^{i\delta_0}\left(\alpha_1+\alpha_2 m_{\pi\pi}^2\right)+\cos\delta_0 e^{i\delta_0}\left(\alpha_3+\alpha_4 m_{\pi\pi}^2\right), \tag{27}$$

where δ_0 is the s-wave phase shift for $I = 0$ and α_i (i=1, 2, 3, 4) are empirical constants to be obtained from data. The first term is due to "compact source" production of the pion pair (see Eq. 5 from Ref. [33]) and the second term is due to production due to an "extended source," for example pion rescattering (see Eq. 5 from Ref. [34] and Eq. 9 from Ref. [35]). We use the parameterization for the s-wave phase shifts from Appendix D of Ref. [36]:[8]

$$\tan\delta_0 \;=\; \frac{2k}{m_{\pi\pi}}\left(A_0^0+B_0^0k^2+C_0^0k^4+D_0^0k^6\right)\left(\frac{4m_\pi^2-s_0^0}{M_{\pi\pi}^2-s_0^0}\right), \tag{28}$$

where we use the same notation as the reference with A_0^0 =0.225, B_0^0 =12.651 GeV^{-2}, C_0^0= -43.8454 GeV^{-4}, D_0^0=-87.1632 GeV^{-6}, and s_0^0=0.715311 GeV^2. We have converted the constants to units of GeV and evaluated the parameters for $a_0^0 = 0.225\, m_\pi^{-1}$, and $a_0^2 = -0.0371\, m_\pi^{-1}$. These fits are only valid below $m_{\pi\pi} < 0.9$ GeV because they do not properly include the $f_0(980)$.

The empirical constants in Eq. 27 were determined by fitting $|\mathcal{A}_W|^2$ to the S-wave contribution to the photoproduction cross section[9] measured by CLAS for $E_\gamma = 3{-}3.8$ GeV [27] for $-t = 0.4{-}0.5$ GeV^2. The fits are for $m_{\pi\pi} = 0.3{-}0.95$ GeV, which is our region of interest. All four parameters are needed to obtain a good representation to the central values of the data, although the uncertainty band in the data allow for a wide range of parameters. Assuming that the constants are real and relatively independent of energy and $-t$, we take the average of the fitted constants for our parameterization ($\alpha_1 = 8.4 \pm 1.4$, $\alpha_2 = -4.1 \pm 2.2$, $\alpha_3 = 2 \pm 1.1$, $\alpha_4 = 8 \pm 1.1$).

[8] See also Eq. 44 of Ref. [33].

[9] The data are available through the Durham HEP Databases, http://durpdg.dur.ac.uk/.

C Angular distribution in the helicity basis

C.1 Photon density matrix in the helicity basis

The linear polarization of the photon can be expressed as (Ref.[37] Eq. 18-19):

$$\begin{aligned} \rho(\gamma) &= \tfrac{1}{2} I + \tfrac{1}{2} \vec{P}_\gamma \cdot \vec{\sigma}, \text{ where} & (29) \\ \vec{P}_\gamma &= \mathcal{P}(-\cos 2\phi_{\pi\pi}, -\sin 2\phi_{\pi\pi}, 0) & (30) \end{aligned}$$

and $\vec{\sigma}$ are the Pauli matrices. The angle $\phi_{\pi\pi}$ is the angle between the polarization vector of the photon and the production plane and $\mathcal{P}$ represents the degree of linear polarization. Multiplying out these factors gives the expression for the photon density matrix in the helicity frame as (Ref.[38] Eq. 219):

$$\rho_{\epsilon,\epsilon'}(\gamma) = \tfrac{1}{2} \begin{pmatrix} 1 & -\mathcal{P} e^{-2i\phi_{\pi\pi}} \\ -\mathcal{P} e^{2i\phi_{\pi\pi}} & 1 \end{pmatrix} \quad (31)$$

C.2 Parity constraints

We consider the reaction $a + b \to c + d$, where the spin of each particle is denoted by s_j, their helicity by λ_j and their intrinsic parity by η_j. If parity is conserved, there are relations between amplitudes with opposite helicities, which are given in Jacob and Wick [39] Eq. 43 and Ref.[37] Eq. 20 [10] (see also Ref. [40] Eq. 4.2.3):

$${}^{\lambda_a} V^{\lambda_d \lambda_b}_{\lambda_c} = \left(\frac{\eta_c \eta_d}{\eta_a \eta_b} \right) (-1)^{s_c + s_d - s_a - s_b} (-1)^{(\lambda_c - \lambda_d) - (\lambda_a - \lambda_b)} \ {}^{-\lambda_a} V^{-\lambda_d - \lambda_b}_{-\lambda_c} \quad (32)$$

C.3 S-wave production

For the case of S-wave production of two pions via the $f_0(500)$ or σ meson off an spinless target we have the following constraint:

$${}^{\lambda_\gamma} V^{\lambda_Z \lambda_Z}_{\lambda_\sigma} = {}^{\epsilon} V^{00}_0 = \left(\frac{\eta_c +}{- +} \right) (-1)^1 (-1)^{-1} \ {}^{-\epsilon} V^{00}_0 = -\eta_c \ {}^{-\epsilon} V^{00}_0 \quad (33)$$

For convenience, we have separated out the parity of the scattered state η_c. The 2π intensity distribution (see Ref.[38] Eq. 220-223 and also Eqs. 264) is given by the following expression after

[10] We thank Adam Szczepaniak for clarifying the connection between these papers.

dropping the superscripts related to the target helicities and collapsing the sums over external and internal spins because both the target and resonance are 0^+ objects:

$$\mathcal{I} = \sum_{\epsilon\epsilon'} {}^{\epsilon}V_0\, Y_0^0\, \rho_{\epsilon\epsilon'}\, {}^{\epsilon'}V_0^*\, Y_0^{0*} \tag{34}$$

$$= \tfrac{1}{2}|Y_0^0|^2 \left({}^1V_0 \quad {}^{-1}V_0\right) \begin{pmatrix} 1 & -\mathcal{P}e^{-2i\phi_{\pi\pi}} \\ -\mathcal{P}e^{2i\phi_{\pi\pi}} & 1 \end{pmatrix} \begin{pmatrix} {}^1V_0^* \\ {}^{-1}V_0^* \end{pmatrix} \tag{35}$$

$$= \tfrac{1}{2}|Y_0^0|^2 \left[|{}^1V_0|^2 - \mathcal{P}\,{}^1V_0\,{}^{-1}V_0^*\, e^{-2i\phi_{\pi\pi}} - \mathcal{P}\,{}^1V_0^*\,{}^{-1}V_0\, e^{2i\phi_{\pi\pi}} + |{}^{-1}V_0|^2\right] \tag{36}$$

Noting that ${}^1V_0 = -\eta_c\,{}^{-1}V_0$, we obtain the following expression:

$$\mathcal{I} = \tfrac{1}{4\pi}|{}^1V_0|^2\,(1 + \eta_c\mathcal{P}\cos 2\phi_{\pi\pi})\,, \tag{37}$$

where $\phi_{\pi\pi}$ is the angle of the polarization vector relative to the production plane. For the case of σ production, $\eta_c = +1$, but for the case of π^0 production we have the opposite sign, $\eta_c = -1$. For the Primakoff production of $\pi^+\pi^-$ in S-wave, $\eta_c = (-1)(-1)(-1)^0 = +1$. See Ref. [1] Eq. 8.

The intensity distribution in Eq. 34 may be written in a more convenient form for use with AmpTools, namely

$$\mathcal{I} = (\tfrac{1-\mathcal{P}}{4})|A_+|^2 + (\tfrac{1+\mathcal{P}}{4})|A_-|^2 \tag{38}$$

$$A_\pm = Y_0^0({}^1V_0 \pm {}^{-1}V_0\, e^{2i\phi_{\pi\pi}}) \tag{39}$$

$$A_\pm = Y_0^0\,{}^1V_0\,(1 \mp \eta_c\, e^{2i\phi_{\pi\pi}}), \tag{40}$$

which can be written more symmetrically taking advantage of an arbitrary phase as

$$A_\pm = Y_0^0\,{}^1V_0\,(e^{-i\phi_{\pi\pi}} \mp \eta_c\, e^{i\phi_{\pi\pi}}). \tag{41}$$

D Scale factors for Primakoff, nuclear coherent, and nuclear incoherent cross sections

Fig. 14 shows ^{208}Pb data from the PrimEx experiment [23]. NPP will run on the same target and the same approximate incident beam energy, ≈ 6 GeV, as PrimEx. Using known analytical forms for the processes shown in the figure, known photo-nuclear cross sections, and estimates for nuclear attenuation from the PrimEx ^{208}Pb analysis, we estimate numerical factors for scaling the Primakoff, nuclear coherent and nuclear incoherent total cross sections seen in PrimEx to the conditions for NPP.

D.1 Scale factor for the Primakoff cross section

The standard equation for Primakoff π^0 production is given by:

$$\frac{d^2\sigma_{PrimEx}}{d\Omega} = \Gamma_{\pi^0\to\gamma\gamma}\frac{8\alpha Z^2}{M_\pi^3}\frac{\beta^3 E_\gamma^4}{Q^4}F_{EM}^2(Q^2)sin^2\theta$$

where $\Gamma_{\pi^0\to\gamma\gamma} = 7.7$ eV is the π^0 radiative width. The cross section for Primakoff $\pi\pi$ production with $P_\gamma = 0$ is given by:

$$\frac{d^2\sigma_{NPP}}{d\Omega_{\pi\pi}dM_{\pi\pi}} = \frac{2\alpha Z^2}{\pi^2}\frac{E_\gamma^4\beta^2}{M_{\pi\pi}}\frac{sin^2\theta}{Q^4}F_{EM}^2(Q^2)\sigma(\gamma\gamma\to\pi\pi)$$

The above equation can be reorganized so that it has a structure similar to the standard Primakoff equation:

$$\frac{d^2\sigma_{NPP}}{d\Omega_{\pi\pi}} \approx \Big[\frac{1}{4\pi^2}\frac{M_{\pi\pi}^2}{\beta}\sigma(\gamma\gamma\to\pi\pi)\Delta M_{\pi\pi}\Big]\frac{8\alpha Z^2}{M_{\pi\pi}^3}\frac{\beta^3 E_\gamma^4}{Q^4}F_{EM}^2(Q^2)sin^2\theta$$

$$\frac{d^2\sigma_{NPP}}{d\Omega_{\pi\pi}} \approx \Gamma_{\pi^0\pi^0\to\gamma\gamma}\frac{8\alpha Z^2}{M_{\pi\pi}^3}\frac{\beta^3 E_\gamma^4}{Q^4}F_{EM}^2(Q^2)sin^2\theta$$

where $\Gamma_{\pi^0\pi^0\to\gamma\gamma}$ is the effective radiative width for $\pi^0\pi^0\to\gamma\gamma$,

$$\Gamma_{\pi^0\pi^0\to\gamma\gamma} = \Big[\frac{1}{4\pi^2}\frac{M_{\pi\pi}^2}{\beta}\sigma(\gamma\gamma\to\pi\pi)\Delta M_{\pi\pi}\Big]$$

Taking $M_{\pi\pi}\approx 0.4$ GeV, $\Delta M_{\pi\pi}\approx 0.4$ GeV, and $\sigma(\gamma\gamma\to\pi^0\pi^0)\approx 10$ nb gives,

$$\Gamma_{\pi^0\pi^0\to\gamma\gamma}\approx 42\ eV$$

The angular dependence of the Primakoff differential cross section for single and double-pion production is given by,

$$\frac{d\sigma}{d\Omega}\sim\frac{sin^2\theta}{Q^4}|F(Q^2)|^2$$

It can be shown (see notes from R. Miskimen) that the peak of the Primakoff differential cross section is at the angle,

$$\theta_{max} = \frac{s}{2E_\gamma^2}$$

where s is the invariant mass squared of the π or $\pi\pi$ system.

The total cross section is given by the integral

$$\sigma\sim\int_0^\Theta\frac{sin^2\theta}{Q^4}|F(Q^2)|^2 2\pi sin\theta d\theta$$

where Θ is the upper integration limit. Working in the small angle limit the total cross section is,

$$\sigma\sim 2\pi\int_0^\Theta\frac{\theta^3}{\left(\frac{s^2}{4E_\gamma^2}+E_\gamma^2\theta^2\right)^2}\Big[1-\frac{1}{6}<r^2>_{charge}\left(\frac{s^2}{4E_\gamma^2}+E_\gamma^2\theta^2\right)+...\Big]^2 d\theta$$

$$\sigma \sim 2\pi \int_0^{\Theta} \frac{\theta^3}{\left(\frac{s^2}{4E_\gamma^2} + E_\gamma^2\theta^2\right)^2}\Big[1 - \frac{1}{3} < r^2 >_{charge} \left(\frac{s^2}{4E_\gamma^2} + E_\gamma^2\theta^2\right)\Big] d\theta$$

Setting $\Theta = C\theta_{max}$ the integral can be evaluated giving,

$$\sigma \sim \frac{\pi}{E_\gamma^4}\left[\Big(ln(1+C^2) - \frac{C^2}{1+C^2}\Big) - \frac{s^2}{4E_\gamma^2}\frac{< r^2_{charge} >}{3}\Big(C^2 - ln(1+C^2)\Big)\right]$$

The integrand in the integral goes through zero at

$$\theta_{min} \approx \frac{1}{E_\gamma}\sqrt{\frac{3}{< r^2 >_{charge}}}$$

provded that,

$$\frac{1}{3} < r^2 >_{charge} \frac{s^2}{4E_\gamma^2} << 1$$

which is valid for CPP and NPP. The angle θ_{min} is approximately the first minimum of the nuclear charge form factor. Setting the upper limit of integration to $\Theta = C\theta_{max} = \theta_{min}$ gives

$$C = \frac{2E_\gamma}{s}\sqrt{\frac{3}{< r^2 >_{charge}}}$$

$$\sigma \sim \frac{\pi}{E_\gamma^4}\left[\Big(ln(1+C^2) - \frac{C^2}{1+C^2}\Big) - \Big(1 - \frac{1}{C^2}ln(1+C^2)\Big)\right]$$

The $1/E_\gamma^4$ factor cancels the E_γ^4 in the Primakoff equation, and therefore the energy dependence of the integrated cross section is relatively weak, given by the dependence of the above equation on $E_\gamma \sim C$.

For the $\pi\pi(\pi)$ final state C = 4.7 (40.8), and the ratio of integrals for double pion to single pion Primakoff production is approximately $I_{\pi\pi}/I_\pi \approx 0.24$ The final result for the ratio of Primakoff cross sections $\sigma_{\pi^0\pi^0}$ to σ_{π^0} is given by,

$$\sigma_{\pi^0\pi^0}\Big/\sigma_{\pi^0} \approx \Big(\Gamma_{\pi^0\pi^0\to\gamma\gamma}\Big/\Gamma_{\gamma\gamma}\Big) \times \Big(M_\pi\Big/M_{\pi\pi}\Big)^3 \times \Big(I_{\pi\pi}\Big/I_\pi\Big) \approx 0.050 \qquad (42)$$

D.2 Scale factor for the nuclear coherent cross section

The nuclear coherent cross section for π^0 photo-production is given by:

$$\frac{d\sigma_{\gamma A\to A\pi^0}}{dt} \approx \eta A^2 \frac{d\sigma_{\gamma N\to N\pi^0}}{dt} sin^2\theta F^2(t)$$

where η is the nuclear absorption factor for π^0 production, A is the atomic mass number, $d\sigma_{\gamma N\to N\pi^0}/dt$ is the π^0 photo-production cross section on the nucleon, and $F(t)$ is the nuclear matter formfactor. The nuclear coherent cross section for $\pi^0\pi^0$ photo-production has a similar form:

$$\frac{d\sigma_{\gamma A\to A\pi^0\pi^0}}{dt} \approx \eta^2 A^2 \frac{d^2\sigma_{\gamma N\to N\pi^0\pi^0}}{dtdM_{\pi\pi}} \Delta M_{\pi\pi} sin^2\theta F^2(t)$$

where $d^2\sigma_{\gamma\to N\pi^0\pi^0}/dtdM_{\pi\pi}$ is the $\pi^0\pi^0$ photo-production cross section on the nucleon. In the near threshold region the dominant channel for $\pi^0\pi^0$ is through $f_0(500)$ photo-production. Cross sections for $f_0(500)$ have been measured in $\gamma p \to \pi^+\pi^-$ at 3.6-3.8 GeV [27]. The s-wave t and $M_{\pi^+\pi^-}$ distributions are shown in Fig. 30, the former at $M_{\pi\pi} = 0.4$ GeV, and the latter at $t = 0.5GeV^2$. Note that $d\sigma^2/dtdM_{\pi^+\pi^-}$ is relatively flat versus $M_{\pi\pi}$ in the threshold region. The relevant cross section for this analysis is $d\sigma^2/dtdM_{\pi^+\pi^-}|_{t=0} \approx 1.0\mu b/GeV^3$ multiplied by an isospin factor of 1/2 to account for the $f_0(500)$ branching fraction to $\pi^0\pi^0$, giving $d\sigma_{\gamma N\to N\pi^0\pi^0}/dtdM_{\pi\pi} \approx 0.5\mu b/GeV^2$. The cross section for $\gamma p \to p\pi^0$ at 6 GeV has been measured at SLAC [41], with cross sections shown in Fig. 31; $d\sigma/dt|_{t=0} \approx 1.5\mu b/GeV^2$. Estimates from the PrimEX ^{208}Pb analysis give $\eta \approx 0.55$.

Assuming an exponential behavior for the differential cross section on the nucleon,

$$\frac{d\sigma_{\gamma N\to NX}}{dt} = \sigma_0 e^{-kt}$$

the coherent angular distribution is given by

$$\frac{d\sigma_{coherent}}{d\Omega} = \sigma_0 sin^2\theta |F(t)|^2 e^{-kt} \frac{dt}{d\Omega}$$

For CPP and NPP we have,

$$\frac{2k}{< r^2 >_{matter}} << 1$$

and

$$\frac{1}{6} < r^2 >_{matter} \frac{s^2}{4E_\gamma^2} << 1$$

Then to leading order in θ^2 the peak coherent cross section is at angle

$$\theta_{max} = \frac{1}{E_\gamma}\sqrt{\frac{2}{< r^2 >_{matter}}}$$

The total cross section is given by,

$$\sigma_{coherent} \sim \sigma_0 \int_0^{C\theta_{max}} sin^2\theta |F(t)|^2 e^{-kt} \frac{dt}{d\Omega} 2\pi sin\theta d\theta$$

where C is a dimensionless scale parameter. Working in the small angle approximation and using the condition,

$$k(\frac{s^2}{4E_\gamma^2}) << 1$$

we can reduce the total cross section to this form,

$$\sigma_{coherent} \sim \frac{8\sigma_0}{< r^2_{charge} >^2 E_\gamma^2} \int_0^C y^3 \Big[1 - \frac{1}{3}y^2\Big]^2 dy$$

Since the integral depends only on C, the integral cancels out in taking the ratio $\sigma_{\gamma A \to A\pi^0\pi^0} \Big/ \sigma_{\gamma A \to A\pi^0}$.

Here we give our final result for the ratio of $\pi^0\pi^0$ to π^0 coherent cross sections:

$$\sigma_{\gamma A \to A\pi^0\pi^0} \Big/ \sigma_{\gamma A \to A\pi^0} \approx \eta \frac{d^2\sigma_{\gamma N \to N\pi^0\pi^0}}{dt dM_{\pi\pi}} \Delta M_{\pi\pi} \Big/ \frac{d\sigma_{\gamma N \to N\pi^0}}{dt} \approx 0.07$$

D.3 Scale factor for the nuclear incoherent cross section

The incoherent cross section for π^0 photo-production is given by:

$$\frac{d\sigma_{\gamma A \to \pi^0}}{dt} \approx \eta A \Big(1 - G(t)\Big) \frac{d\sigma_{\gamma N \to N\pi^0}}{dt}$$

where G(t) is a Pauli suppression factor, with G(0)=1 and $G(t) \to 0$ for $t > k_F$, where k_F is the nuclear Fermi momentum, $k_F \approx 260$ MeV/c. The incoherent cross section for $\pi^0\pi^0$ photo-production has a similar form:

$$\frac{d\sigma_{\gamma A \to \pi^0\pi^0}}{dt} \approx \eta^2 A \Big(1 - G(t)\Big) \frac{d^2\sigma_{\gamma N \to N\pi^0\pi^0}}{dt dM_{\pi\pi}} \Delta M_{\pi\pi}$$

The photo-production cross sections on the nuclon are identical to those used in the estimation of the coherent cross section.

The total cross section is given by,

$$\sigma \sim \sigma_0 \int_{s^2/4E_\gamma^2}^{CE_\gamma^2\theta^2_{max}} \Big(1 - G(t)\Big) e^{-kt} dt$$

where we integrate up to a multiple of $E_\gamma^2\theta^2_{max}$, where θ_{max} is the angle of the peak coherent cross section, and $s^2/4E_\gamma^2$ is the minimum t in the reaction. Because $s^2/4E_\gamma^2 << k_F^2$ and $1 - G(s^2/4E_\gamma^2) \approx 0$, the lower limit on the integral can be replaced with zero,

$$\sigma \sim \int_0^{CE_\gamma^2\theta^2_{max}} \Big(1 - G(t)\Big) e^{-kt} dt$$

For π or $\pi\pi$ photo-production

$$CE_\gamma^2\theta_{max}^2 k \approx C\frac{2}{< r^2 >_{matter}}k << 1$$

provided that $C \leq 5$. In this case we can neglect the exponential in the integral,

$$\sigma \sim \int_0^{CE_\gamma^2\theta_{max}^2} \Big(1 - G(t)\Big)dt$$

Since the integral depends only on the upper integration limit, the integral cancels out in taking the ratio $\sigma_{\gamma A\to\pi^0\pi^0}\Big/\sigma_{\gamma A\to\pi^0}$. Our final result for the ratio of $\pi^0\pi^0$ to π^0 incoherent cross sections is given by:

$$\sigma_{\gamma A\to\pi^0\pi^0}\Big/\sigma_{\gamma A\to\pi^0} \approx \eta\frac{d^2\sigma_{\gamma N\to N\pi^0\pi^0}}{dtdM_{\pi\pi}}\Delta M_{\pi\pi}\Big/\frac{d\sigma_{\gamma N\to N\pi^0}}{dt} \approx 0.07$$

D.4 Summary

NPP will take data on the same target, ^{208}Pb, and the same approximate incident beam energy, ≈ 6 GeV, as PrimEx. Using known analytical expressions for the Primakoff, nuclear coherent, and nuclear incoherent cross sections, known photo-nuclear cross sections, and estimates for nuclear attenuation from the PrimEx ^{208}Pb analysis, numerical factors are calculated for scaling the total cross sections seen in PrimEx to the conditions for NPP. Assuming $M_{\pi^0\pi^0} \approx 0.4$ GeV, and a width $\Delta M_{\pi^0\pi^0} \approx 0.4$ GeV, the scale factors for Primakoff, nuclear coherent, and nuclear incoherent total cross sections are approximately $\times 0.05$, $\times 0.07$, and $\times 0.07$, respectively.

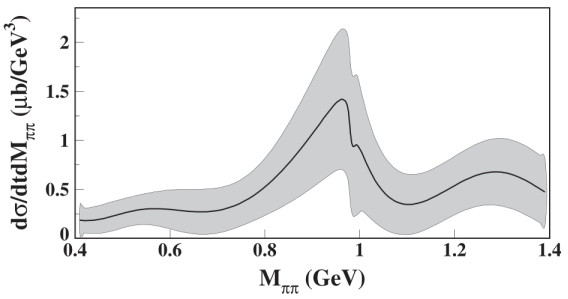

S-wave cross section derived by the fit in the $3.2 < E_\gamma < 3.4$ GeV and $0.5 < -t < 0.6$ GeV^2 bin. The systematic and the fit uncertainties are added in quadrature and are shown by the gray band.

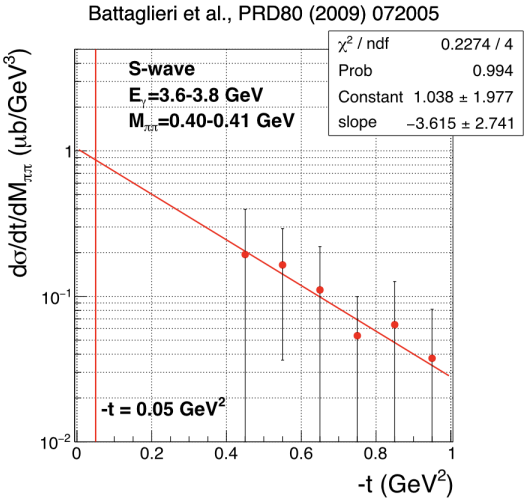

Figure 30: CLAS data for s-wave $\pi^+\pi^-$ photoproduction on the proton at $3.2 < E_\gamma < 3.4$ GeV [27].

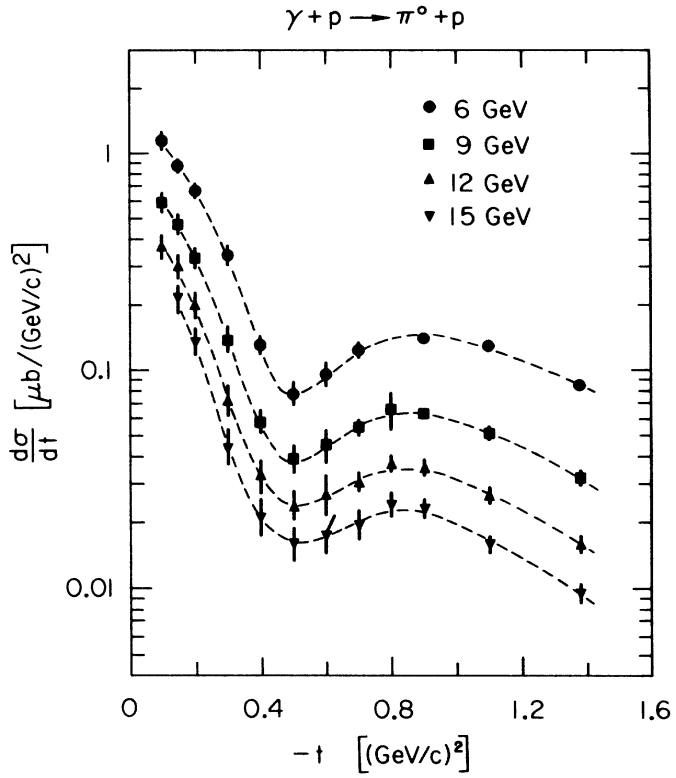

Fig. 5. $d\sigma/dt$ in μb/(GeV/c)^2 is plotted versus $|t|$ for incident photon energies of 6, 9, 12, and 15 GeV. The dashed lines are only to guide the eye.

Figure 31: SLAC data for π^0 photo-production on the proton [41].